medicina

MDPI

Review

Novel Molecular Classification of Breast Cancer with PET Imaging

Ngô Minh Toàn [1,2]

[1] Gyula Petrányi Doctoral School of Clinical Immunology and Allergology, Faculty of Medicine, University of Debrecen, H-4032 Debrecen, Hungary; ngo@mailbox.unideb.hu
[2] Medical Imaging Clinic, Clinical Centre, University of Debrecen, H-4032 Debrecen, Hungary

Abstract: Breast cancer is a heterogeneous disease characterized by a wide range of biomarker expressions, resulting in varied progression, behavior, and prognosis. While traditional biopsy-based molecular classification is the gold standard, it is invasive and limited in capturing tumor heterogeneity, especially in deep or metastatic lesions. Molecular imaging, particularly positron emission tomography (PET) imaging, offering a non-invasive alternative, potentially plays a crucial role in the classification and management of breast cancer by providing detailed information about tumor location, heterogeneity, and progression. This narrative review, which focuses on both clinical patients and preclinical studies, explores the latest advancements in PET imaging for breast cancer, emphasizing the development of new tracers targeting hormone receptors such as the estrogen alpha receptor, progesterone receptor, androgen receptor, estrogen beta receptor, as well as the ErbB family of receptors, VEGF/VEGFR, PARP1, PD-L1, and markers for indirectly assessing Ki-67. These innovative radiopharmaceuticals have the potential to guide personalized treatment approaches based on the unique tumor profiles of individual patients. Additionally, they may improve the assessment of treatment efficacy, ultimately leading to better outcomes for those diagnosed with breast cancer.

Keywords: breast cancer; positron emission tomography; PET biomarkers

Citation: Toàn, N.M. Novel Molecular Classification of Breast Cancer with PET Imaging. *Medicina* **2024**, *60*, 2099. https://doi.org/10.3390/medicina60122099

Academic Editor: Konstantinos Dimas

Received: 15 November 2024
Revised: 13 December 2024
Accepted: 19 December 2024
Published: 21 December 2024

1. Introduction

Breast cancer remains a significant global health concern, with about 2.2 million new cases and 685,000 deaths reported in 2020 [1]. The risk of developing breast cancer escalates with age, particularly affecting individuals between the ages of 60 and 69 [2]. Despite improving trends in breast cancer mortality rates, there has been a rapid increase in incidence, particularly in developed countries [1].

To effectively address the increasing burden of breast cancer, it is crucial to investigate the disease at a molecular level. Breast cancer is classified into four molecular subtypes: Luminal A, Luminal B, HER2-enriched, and Triple-Negative Breast Cancer (TNBC). This classification is based on the positivity of receptors (estrogen, progesterone, and HER2 receptors) and the level of Ki67 [3]. Each subtype has distinct risk factors [4], prevalence patterns [2,5], and treatment plans. In addition to variances in surgical and radiation approaches, the chemotherapeutic treatment of each breast cancer subtype also differs; hormone-positive subtypes typically respond to endocrine therapy, HER2-positive subtypes require HER2-targeted therapy, and TNBC relies on cytotoxic agents [3]. These differences may lead to different adverse effect profiles of the chemotherapy and differences in medical expenses [6,7]. Furthermore, the behavior and prognosis of each subtype vary. Luminal A tumors generally have the highest survival rates, whereas TNBC is characterized by aggressiveness and a greater tendency to metasta-

size to the brain and lungs, unlike other subtypes, which may also metastasize to the liver [8,9].

Traditionally, molecular classification relied on biopsy-based samples using methods like immunohistochemistry (IHC) or fluorescent in situ hybridization (FISH). However, these approaches are invasive, uncomfortable, and cannot effectively access deep or metastatic lesions. Cancer cells undergo genetic mutations and cellular changes that drive progression, adaptation, and drug resistance. These mutations accumulate, creating genetic diversity and tumor heterogeneity [10]. Breast cancer exhibits significant levels of tumor heterogeneity, influencing therapy sensitivity and patient overall survival [11]. Even though it is considered the gold standard, tissue-based sampling has intrinsic limitations in accessing both intra-tumor and inter-tumor heterogeneity, particularly considering the complexity and progression of breast neoplasms [12].

Imaging methods have been implemented to classify the breast cancer subtypes using different patterns observed in many ultrasound, MRI, and CT techniques [13–17]. Moreover, [^{18}F]Fluorodeoxyglucose (FDG) studies have revealed significant metabolic variations between luminal and non-luminal subtypes [18]. Additionally, studies implemented angiogenesis Arginylglycylaspartic acid (RGD) imaging to classify the subtypes better, using a metabolic activity-to-angiogenesis ratio [19,20]. These approaches are based on the distinct behaviors observed across the subtypes: luminal subtypes exhibit a higher rate of desmoplastic reaction, while non-luminal subtypes, particularly TNBC, are more aggressive, with increased metabolism and frequent central necrosis. The HER2-enriched subtype shows heightened angiogenesis. However, these imaging techniques are nonspecific and cannot accurately determine tumor receptor status and molecular subtypes with high confidence.

With recent attention and advancements, Positron Emission Tomography (PET) molecular imaging has emerged as a promising tool for assessing breast cancer biomarkers thanks to its high quantitative ability and resolution [21]. Furthermore, numerous additional biomarkers (EGFR, HER3, VEGF, androgen receptors, etc.) have been identified as playing significant roles in treatment options and prognosis, supplementing the conventional classifications.

Molecular imaging of breast cancer enables whole-body, non-invasive investigation of receptor statuses and other molecular biomarkers using novel radiopharmaceuticals. These biomarkers can change, particularly during metastasis or after treatment, complicating prognosis. Molecular imaging can dynamically track these changes, providing critical insights into tumor heterogeneity, subtype-specific characteristics, and cancer behavior patterns, thus allowing the precise identification of subtypes and biomarkers, guiding timely targeted therapies that maximize efficacy while minimizing side effects.

This narrative review summarizes the latest advancements in molecular imaging for breast cancer classification, targeting both conventional (Table 1) and novel biomarkers (Table 2) in tumor and infiltrating immune cells (Figure 1). We specifically focus on the most recent radiotracers and their application from preclinical research to clinical settings. These advancements have the potential to optimize therapy selection and monitor therapy responses, ultimately improving personalized treatment strategies in the future.

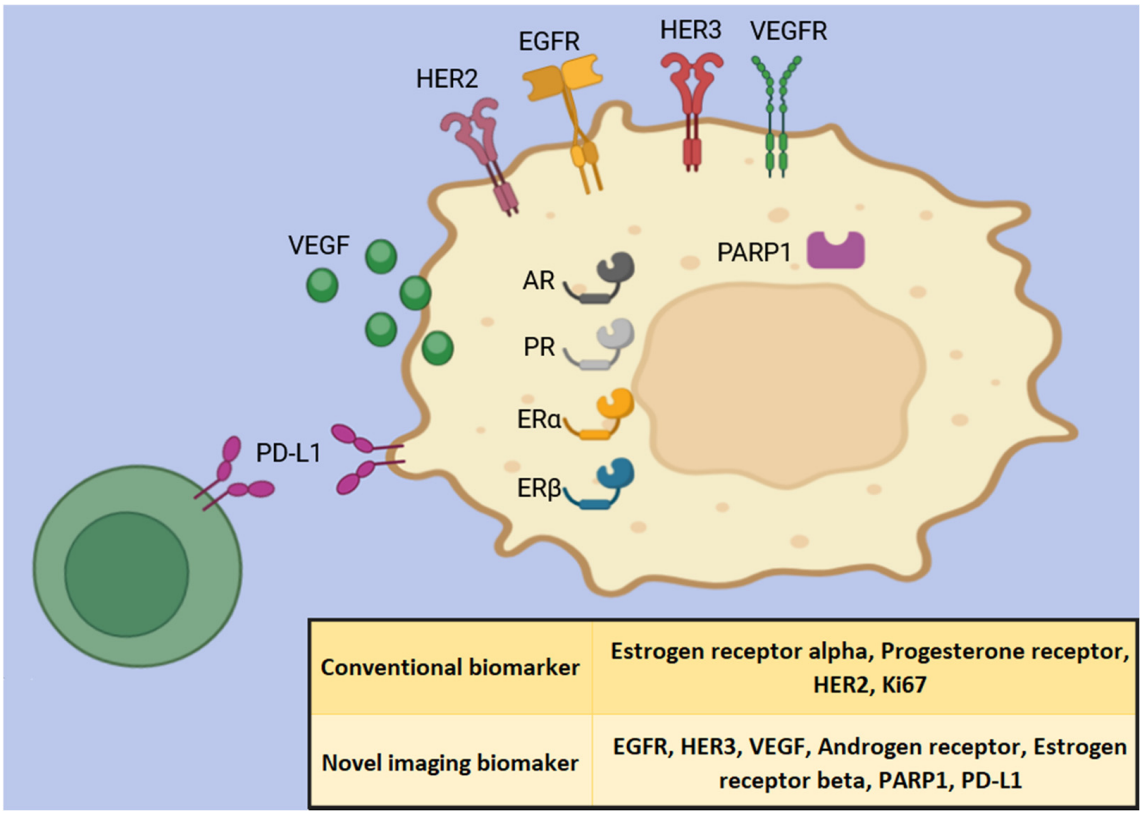

Figure 1. An overview of the imaging targets for breast imaging discussed in this review. The green, smaller cell in the bottom-left corner represents a white blood cell, while the larger, orange cell on the right represents a breast cancer cell. This figure was created with BioRender.com.

2. Conventional Biomarkers Imaging

2.1. Human Epidermal Growth Factor Receptor 2 Imaging

Human epidermal growth factor receptor 2 is one of the receptors in the epidermal growth factor family, encoded by the erbB-2 oncogene. Its protein overexpression or gene amplification has been present in around one-fifth of breast cancer cases [22], especially in HER2-enriched or HER2+ luminal B subtypes, which have a worse prognosis than their HER2-negative counterpart [23]. Upon dimerization, the receptor initiates tyrosine kinase activity and a cascade of events that regulate cell proliferation and angiogenesis, promoting cancer invasion and metastasis [22]. Consequently, HER2-positive breast cancer has a higher risk of metastasis, with a predilection to spread to the bone, liver, and brain [24]. Even though many HER2 targeting therapies have shown promising results, HER2 breast cancer heterogeneity is a significant challenge in treating breast cancer patients. There is around a 28% conversion rate in HER2 status between primary tumors and subsequent recurrent or metastatic lesions, representing inter-tumor heterogeneity [25]. Furthermore, HER2 intra-tumor heterogeneity also plays a crucial role in therapy resistance and poor prognosis [26,27]. Recently, the HER2-low subtype (IHC +1 or IHC +2 with negative FISH) has been classified, requiring a distinct approach, with first-line therapy relying on trastuzumab deruxtecan and necessitating a dedicated assessment of HER2 levels [28]. Therefore, HER2 imaging offers a non-invasive method to assess the HER2 status of both primary tumors and metastases, as well as heterogeneity status, thus helping in therapy selection, predicting, and following up on therapy response.

2.1.1. Trastuzumab Labeled with ^{89}Zr

The use of the radiolabeled isotope ^{89}Zr, with an extended half-life of approximately 78 h, is effective for labeling antibodies (also with long biological half-life). Trastuzumab labeled with ^{89}Zr using the chelator DFO has been extensively evaluated in clinical settings. In most trials, it is common practice to administer a "cold" dose of trastuzumab, typically around 50 mg, prior to the tracer injection to reduce background signal. Scanning is usually performed 4 to 5 days after tracer administration [29,30]. However, studies suggest a lower cold dose may be more appropriate for patients already undergoing trastuzumab treatment [31]. The [^{89}Zr]Zr-DFO-trastuzumab tracer has demonstrated its ability to detect or monitor HER2 status in metastatic lesions in the liver, bone, and lymph nodes regardless of the HER2 status of the primary tumor [29–31]. Notably, it can also detect brain metastases, likely due to tracer uptake facilitated by the disruption of the blood-brain barrier [32].

Despite these promising results, there is a recognized risk of discordance between the tracer uptake and IHC results, particularly in bone, liver, and lymph node lesions [33]. This discrepancy may lead to false positives, primarily attributed to the instability of DFO as a chelator for ^{89}Zr. The free zirconium that is released tends to accumulate in bone tissue. Moreover, Fc-mediated uptake in active lymph nodes and the liver—key sites of antibody metabolism—can also result in false positives.

The tracer's potential in following up therapy responses was demonstrated by Linders et al., using different parameters and ΔSUV_R (the difference between SUV ratios before and after therapy). However, the study included a small number of patients (n = 6) and reported some false-negative cases (two cases) likely due to HER2 downregulation following high-dose trastuzumab [34]. In larger clinical trials (e.g., the ZEPHIR trial), combining [^{89}Zr]Zr-DFO-trastuzumab imaging with conventional FDG PET/CT significantly improved the ability to predict treatment response to trastuzumab emtansine (T-DM1), achieving positive predictive values (PPV) and negative predictive values (NPV) exceeding 90%, up to 100% [35,36]. Furthermore, a clinical trial by Gaykema et al. showed that [^{89}Zr]Zr-DFO-trastuzumab imaging can help predict treatment responses when used alongside heat shock protein 90 (HSP90) inhibitors in patients. The results showed significant correlations between the ΔSUV_{max} and decrease in tumor size (r^2 = 0.69) [37]. Additionally, in a preclinical study by McKnight et al. involving breast cancer tumor-bearing mice, the tracer was able to assess the effectiveness of tyrosine kinase inhibitors. There were significant correlations between tumor uptake and decreases in HER2 expression (r around 0.6) and in tumor volume (r around 0.8) [38]. These findings underscore the potential of [^{89}Zr]-DFO-trastuzumab not only in monitoring HER2 status but also in evaluating the efficacy of different therapeutic approaches. Nevertheless, larger studies with standardized assessment methods are required, whether using the SUV_{max} lesion-to-background ratio, blood, liver, or contralateral side.

To address the in vivo instability of DFO, alternative chelators for [^{89}Zr]Zr-DFO-trastuzumab have been developed and tested in preclinical models. For example, Deri et al. showed that HOPO improved stability with lower bone uptake but presented challenges in synthesis and lower tumor uptake [39]. DFO* (DFOstar) was demonstrated by Chomet et al. to significantly improve thermodynamic stability while maintaining similar tumor-to-background ratios (TBRs). This resulted in lower bone uptake and greater accuracy in detecting breast cancer bone metastases [40].

Site-specific conjugation produces a more homogeneous tracer, leading to more predictable specificity and pharmacokinetics. In a study by Vivier et al. involving humanized mice with breast cancer, both fully (by PNGaseF) and partially (by EndoS) deglycosylated antibodies were conjugated to DFO specifically at the heavy chain glycan site ([^{89}Zr]Zr-DFO-^{ss}trastuzumab-EndoS) or non-specifically ([^{89}Zr]Zr-DFO-^{nss}trastuzumab-PNGaseF). Both strategies showed significantly higher tumor uptake and an improved tumor contrast with significantly lower liver and spleen uptake compared to [^{89}Zr]Zr-DFO-trastuzumab [41]. This improvement is attributed to the attenuation of FcγR interactions

while maintaining high HER2 binding affinity, requires additional but facile enzymatic deglycosylation step.

2.1.2. Trastuzumab Labeled with ^{64}Cu

In addition to [^{89}Zr]Zr-DFO-trastuzumab, the use of [^{64}Cu]Cu-DOTA-trastuzumab has also been investigated in patients due to its comparable long half-life of 12.7 h and better resolution due to lower positron energy (0.656 MeV vs. 0.897 MeV) [42]. Studies suggest that administering a cold dose of 50 mg trastuzumab, followed by a 48 h incubation period would optimize the TBR [43]; however, the tracer's tumor visualization was limited in patients undergoing trastuzumab therapy [44]. Like [^{89}Zr]Zr-DFO-trastuzumab, [^{64}Cu]Cu-DOTA-trastuzumab has proven effective in visualizing known brain metastases larger than 1 cm with high confidence and HER2 specificity (validated with IHC and autoradiography) [45]. There is some discordance between FDG PET imaging and [^{64}Cu]Cu-DOTA-trastuzumab, with certain lesions showing positivity with one tracer but not the other [43], suggesting the potential supplementary role of the tracer to the conventional FDG.

Moreover, [^{64}Cu]Cu-DOTA-trastuzumab has demonstrated potential in predicting therapy response in HER2-positive patients. Mortimer et al. showed that patients who responded to treatment exhibited significantly higher baseline uptake at 2 days post-injection compared to non-responders. Although the study's small sample size (n = 10) limits the generalizability of these findings [46].

One challenge with ^{64}Cu is its tendency to transchelate with serum compounds, highlighting the need for a more stable chelator. A preclinical study by Woo et al. showed that [^{64}Cu]Cu-NOTA-trastuzumab offers high specificity (significant tumor uptake decrease when blocked in vivo with cold trastuzumab) and a lower uptake and absorbed dose to organs compared to DOTA, indirectly indicating greater stability [47]. A clinical pilot study using the same tracer by Lee et al. also reported a reduced organ dose and a higher uptake in HER2-positive lesions compared to negative ones [48]. Recently, the NODAGA chelator has emerged as a promising alternative; [^{64}Cu]Cu-NODAGA-trastuzumab offers easier labeling and enhanced stability while retaining high specificity in vitro [49].

2.1.3. Trastuzumab Labeled with ^{52}Mn

With a similar extended half-life of 5.6 days, ^{52}Mn, a promising candidate for antibody-based imaging, offers an attractive radiation profile compared to ^{89}Zr and ^{64}Cu. Its 29% positron emission with a low maximum energy (0.575 MeV) results in enhanced resolution [50]. Toàn et al. utilized BPPA, a bispyclen-based chelator, to label trastuzumab with ^{52}Mn. The resulting tracer, [^{52}Mn]Mn-BPPA-trastuzumab, demonstrated higher TBRs and effectively distinguished HER2-positive from HER2-negative tumors in preclinical models, outperforming [^{52}Mn]Mn-DOTAGA-p-SCN-trastuzumab, though in vivo stability needs further enhancement [51]. Omweri et al. evaluated [^{52}Mn]Mn-Oxo-DO3A-trastuzumab, which showed comparable specific activity to [^{52}Mn]Mn-BPPA-trastuzumab but with improved stability. This tracer accurately evaluated HER2 expression, showing significantly higher tumor-to-muscle ratios in HER2-positive tumors compared to HER2-negative ones in preclinical models [52].

2.1.4. Pertuzumab Labeled with ^{89}Zr

Imaging the HER2 receptor with a trastuzumab-based tracer during trastuzumab therapy can be challenging due to the saturation of the receptor's binding sites. An alternative approach using pertuzumab, which binds to a distinct epitope on HER2, offers a potential solution. In a preclinical study by Marquez et al. using breast cancer xenografts, the [^{89}Zr]Zr-DFO-pertuzumab tracer demonstrated high specificity, with significant tracer uptake observed during trastuzumab therapy [53]. Building on these findings, a patient study (n = 6) by Ulaner et al. revealed that optimal imaging was achieved 5–8 days post-injection with a cold dose of pertuzumab administered beforehand to enhance the

TBR. The approach resulted in a slightly higher absorbed dose compared to [^{89}Zr]Zr-DFO-trastuzumab. Nevertheless, the tracer proved effective in investigating HER2 heterogeneity and was able to detect brain HER2 metastases in some patients [54].

Beyond differentiating HER2 positivity, this tracer has been explored in preclinical models for its ability to follow up and predict therapy response. For instance, after T-DM1 treatment, the tracer visualized changes in HER2-positive tumor size more effectively than FDG. Specifically, the tumor's tracer uptake did not significantly change, which is hypothesized to correspond to the unchanged HER2 concentration post-therapy [55]. In contrast, a study by Kang et al. with HSP90 inhibitor therapy showed decreased HER2 expression and a significant reduction in tumor uptake after treatment [56]. Another study by Lu et al. demonstrated the tracer's predictive ability following paclitaxel treatment, where tumors with higher tracer uptake responded better, exhibiting reduced size and decreased FDG uptake ($r = -0.59$), correlating with lower HER2 expression post-therapy [57]. These findings highlight the tracer's potential not only for characterizing HER2 expression but also for predicting and monitoring dynamic changes in HER2 status.

Similar to [^{89}Zr]Zr-DFO-trastuzumab, a site-specific version, [^{89}Zr]Zr-^{ss}DFO-pertuzumab, developed by Vivier et al., showed improved tumor-to-spleen and liver ratios in preclinical models [58]. In a clinical study (n = 6) by Yeh et al., the site-specific tracer exhibited a similar total absorbed dose compared to non-specific [^{89}Zr]Zr-DFO-pertuzumab, but with the kidney identified as the critical organ instead of the liver. Nevertheless, the site-specific tracer provided better lesion visualization in some HER2-positive patients than the non-specific version [59].

2.1.5. Trastuzumab Emtansine Labeled with ^{89}Zr

Trastuzumab emtansine (T-DM1) is an antibody-drug conjugate effective for some patients with trastuzumab-resistant cancers, but many either fail to respond or develop resistance over time. To improve therapy selection, [^{89}Zr]Zr-DFO-T-DM1 can be employed over [^{89}Zr]Zr-DFO-trastuzumab. In preclinical breast cancer models with varying HER2 expression, Al-Saden et al. demonstrated that this tracer shows high HER2 specificity, comparable to [^{89}Zr]Zr-DFO-trastuzumab, and is particularly effective at stratifying HER2 status at 4 days post-injection [60]. A subsequent study, also in preclinical models using tumor-to-blood ratios, showed that the tracer could classify HER2 expression levels, with very strong correlations with HER2 expression ($r^2 = 0.94$) and, importantly, with tumor response to T-DM1 [61].

2.1.6. Labeled Trastuzumab Fragments

Antibody fragments lacking the Fc region could offer superior alternatives due to their faster pharmacokinetics compared to full-length antibodies. In a study by Suman et al. using F(ab') and F(ab')2 fragments labeled with ^{68}Ga via the NOTA chelator, the fragments retained their affinity, and the labeling process was gentler than with the conventional DOTA chelator, which can damage heat-labile fragments. As expected when using antibody fragments, the F(ab') was primarily eliminated through the kidneys, exhibiting a faster clearance rate and consequently achieving higher tumor-to-organ ratios than F(ab')2, except for the tumor-to-kidney ratios [62].

A study by Moreau et al. on breast cancer tumor-bearing mice, investigating the optimal chelator for the ^{64}Cu labeling of trastuzumab's Fab fragment, found that MANOTA provided better stability and superior tumor-to-blood and tumor-to-liver ratios (around twofold higher) compared to DOTA, DOTAGA, and even the previously mentioned NODAGA, which already had shown some improvements [63].

Various methods for the site-specific labeling of trastuzumab fragments have been explored. For instance, a modified Fab with a mutated light chain containing methionine—a rare amino acid typically hidden within protein pockets—enables easy and specific conjugation, enhancing labeling precision. Implementing the techniques in preclinical models, Yue et al. demonstrated that [^{68}Ga]Ga-DFO-M74 trastuzumab's Fab demonstrated

higher affinity and stability, leading to faster clearance from organs and higher tumor uptake, resulting in an approximately twofold higher tumor-to-background than the wild-type tracer [64].

However, their small size makes antibody fragments rapidly cleared from the body, which may limit tumor uptake. Strategies such as adding polyethylene glycol (PEG) can extend their half-life, although this requires chemical conjugation. An alternative approach, PASylation—the addition of Pro, Ala, and Ser sequences—has been tested in pilot mice models by Mendler et al. [65] and in a human study (n = 1) with HER2-positive breast cancer by Richter et al. [66]. This technique showed prolonged plasma retention and successfully visualized primary tumors and metastases.

2.1.7. HER2 Nanobody

Nanobodies, which are heavy-chain antibodies found in camelids, are even smaller than antibody fragments. HER2-targeting nanobodies, such as 2Rs15d and 5F7, are particularly well-suited for imaging with ^{18}F due to their complementary short half-lives.

Zhou et al. utilized these two nanobodies with the novel fluorine prosthetic TFPFN for HER2-positive breast cancer xenograft imaging. In vitro results showed that [^{18}F]TFPFN-5F7 exhibited a better binding affinity and a higher internalization rate than [^{18}F]TFPFN-2Rs15d. However, 2Rs15d binds to a different domain (domain I) than trastuzumab (domain IV) and pertuzumab (domain II), making it a suitable imaging agent for patients undergoing HER2-targeting antibody therapies, whereas 5F7 binds to domain IV. Nevertheless, in vivo, both tracers showed high specificity for HER2 tumors and lower kidney uptake compared to other available ^{18}F prosthetics. This reduced the radiation dose to the kidneys and improved tumor contrast, achieving tumor visualization comparable to residualizing labels [67]. Due to the similarly short physical half-life, [^{68}Ga]Ga-NOTA-2Rs15d was studied by Gondry et al. and Keyaerts et al. in breast cancer patients, demonstrating good reproducibility, safety, and effectiveness in detecting tumor heterogeneity [68,69]. In a preclinical study by Ducharme et al. involving breast cancer xenografts with varying HER2 expression levels, [^{89}Zr]Zr-DFO-2Rs15d was used to investigate the biodistribution of the nanobody at later time points. The tracer demonstrated high specificity for HER2 and was only partially blocked by trastuzumab in vitro, likely due to the induced internalization after binding. However, while small tracers like nanobodies are primarily cleared through the kidneys, the consistent and prominent kidney uptake observed up to day 3 poses a challenge for dosimetry [70].

2.1.8. HER2 Affibody

Affibody molecules, which are protein scaffolds based on the Z domain of Staphylococcus Protein A, have an even smaller molecular size than nanobodies (just a few kDa) and exhibit exceptionally high affinity for the HER2 receptor (in the pM KD range). ZHER$_{2:342}$ (ABY-002) was the first affibody tested in humans; however, it showed high liver uptake, which could impede the detection of hepatic metastases and necessitate modifications for optimal labeling—potentially altering the tracer's in vivo behavior [71]. To address this, ZHER$_{2:2395}$ was developed with an added cysteine at the C-terminus, increasing labeling possibilities [72]. Further refinement led to ZHER$_{2:2891}$, which includes amino acid substitutions near the C-terminus to improve stability and increase hydrophilicity while retaining high affinity for HER2 [73]; adding a cysteine residue along with a DOTA chelator produces ABY-025.

[^{68}Ga]Ga-ABY-025 has been clinically tested, demonstrating a lower absorbed dose compared to FDG [74] and effectively differentiating HER2 positivity, particularly through the TBR (optimally tumor-to-spleen ratio) [75]. It was also able to detect HER2 heterogeneity [76], which is especially beneficial in HER2-low patients [77]. While the correlation with IHC was not significant [77], the tracer did show a significant correlation with metabolic response to HER2-targeted therapy [78].

To reduce the hepatic uptake of $ZHER_{2:342}$ tracers, Xu et al. developed $MZHER_{2:342}$ by adding a hydrophilic linker and labeling the affibody with different isotopes. In preclinical models, [^{18}F]F-Al-MAL-NOTA-Cys-$MZHER_{2:342}$ successfully demonstrated HER2 specificity and showed a significant correlation with HER2 IHC scores (r^2 = 0.99). This labeling strategy also further decreased liver uptake, along with low bone uptake, indicating enhanced tracer stability; however, kidney uptake remained high [79]. Similarly, [^{68}Ga]Ga-MAL-NOTA-Cys-$MZHER_{2:342}$ was able to differentiate HER2 positivity in patients and showed lower liver uptake compared to ABY-025 [80]. [^{89}Zr]Zr-DFO-MAL-NOTA-Cys-$MZHER_{2:342}$ in tumor-bearing mice also exhibited HER2 specificity, with reduced liver and osseous uptake, further suggesting the tracer's stability [81]. Consequently, this highlights the flexibility and reproducibility of labeling $MZHER_{2:342}$ and its potential for future studies.

Affibody molecules represent a promising approach for HER2 breast cancer imaging, and ongoing developments aim to enhance their performance. Recently, $ZHER_{2:2891}$ was modified to ABY-027 (including an albumin-binding domain) to reduce kidney uptake and tested in preclinical models with [^{177}Lu]Lu-ABY-027 for targeted radionuclide therapy [82]. Additionally, the newer affibody $ZHER_{2:41071}$ features improved stability and hydrophilicity and is currently being evaluated in clinical studies using SPECT imaging with the ^{99m}Tc-$ZHER_{2:41071}$ tracer [83].

2.1.9. Other Scaffolds and Peptides

Similar to affibodies, ADAPT6 (ABD-Derived Affinity ProTein), a scaffold derived from the albumin binding domain (ABD) of streptococcal protein G, can target HER2 with high affinity and rapid clearance. A study using (HE)3DANS-ADAPT6-GSSC labeled with ^{68}Ga by different chelators showed high affinity for HER2-positive breast and ovarian cancer cell lines in vitro. In vivo testing on ovarian cancer-bearing mice revealed that [^{68}Ga]Ga-(HE)3DANS-ADAPT6-GSSC-NODAGA achieved the best TBR (compared to DOTA, DOTAGA, and NOTA variants), highlighting its potential as a promising small molecule for HER2 targeting [84].

Another promising candidate is DARPins (designed ankyrin repeat proteins), small peptides with a high affinity for HER2. [^{89}Zr]Zr-DFO-G3-DARPin, produced by Fay et al. through sortase enzyme site-specific conjugation, despite the slow conjugation process, demonstrated high affinity and specificity with excellent tumor contrast in breast cancer xenograft preclinical models [85].

Protein scaffolds of bacterial origin, or to a lesser extent from camelids, may trigger immunogenic responses [86]. Small synthetic peptides are a promising class of candidates for HER2 imaging due to their ease of modification and reduced immunogenicity. However, these peptides can be degraded by enzymes in vivo, so strategies like D- or beta-amino acid substitution, cyclization, and PEGylation are often employed to enhance their stability [87]. Among the studied peptides, two are particularly notable: KCCYSL, which has a high affinity with a Kd of 295 nM and binds to a different site than trastuzumab, and LTVSPWY, which, while having a lower affinity, binds to the same site as trastuzumab [88]. A study by Biabani et al. using [^{68}Ga]Ga-DOTA-$(Ser)_3$-LTVSPWY to assess HER2-positive breast cancer xenografts in mice showed high tumor affinity, with a significant decrease in uptake when blocked both in vitro and in vivo with an unlabeled peptide. The tracer demonstrated serum and in vivo stability, with rapid renal clearance due to increased hydrophilicity from serine residues. Despite high initial renal activity, uptake decreased rapidly after 1 h, maintaining an adequate tumor-to-blood ratio of 1.7 at 2 h post-injection [89]. Another study by Ducharme et al. compared [^{68}Ga]Ga-DOTA-PEG_2-DTFPYLGWWNPNEYRY and [^{68}Ga]Ga-DOTA-PEG_2-GSGKCCYSL, using phosphoramidon to protect against degradation. Although both tracers demonstrated significant differences between HER2-positive and HER2-negative tumors, the differences were inconsistent across time points (1h versus 2h post-injection) and did not show significant uptake decreases in the in vivo PET blocking study. Nonetheless, [^{68}Ga]Ga-DOTA-PEG_2-DTFPYLGWWNPNEYRY appeared more

promising, with higher tumor uptake at 1 h post-injection and greater stability in human serum [90].

In conclusion, small molecules (nanobodies, affibodies, etc.) targeting HER2 offer significant advantages, including high affinity and rapid clearance, leading to high tumor contrast and lower absorbed doses. However, they commonly suffer from high kidney uptake, prompting various strategies to address this issue, such as administering Gelofusine, adding linkers like PEG or PAS, using non-residualizing chelators or prosthetics, and improving tracer stability [91]. However, these modifications can potentially alter the peptide's function and biodistribution, underscoring the need for further research to develop optimal HER2 imaging agents.

2.2. Estrogen Receptor Alpha Imaging

Estrogen receptor positivity is present in over 60% of breast cancer patients [92], primarily driven by the alpha estrogen receptor, which determines the luminal subtypes [93]. Heterogeneity of estrogen receptor expression is observed in over one-third of advanced estrogen receptor-positive cases [94]. Furthermore, endocrine therapy, commonly used in these patients, can build up cancer resistance through receptor loss [95], receptor gene mutations, or the activation of related pathways, necessitating combination therapies [96]. Therefore, PET imaging that targets the alpha estrogen receptor provides valuable insights into receptor status in both primary tumors and metastases, supporting timely therapy adjustments and monitoring of treatment response.

In ER-positive patients, in comparison with [^{18}F]FDG, imaging using [^{18}F]FES (fluoroestradiol) has demonstrated improved detection of metastases in bone lesions, whereas [^{18}F]FDG is more effective for non-bone lesions. Thus, combining these tracers can enhance metastasis detection and improve staging and re-staging accuracy [97–99].

Furthermore, a study in ER-positive patients by Iqbal et al. showed that [^{18}F]FES can effectively predict response to anti-estrogen therapy, independent of ESR1 mutation status [100]. This tracer tracks changes in ER expression throughout treatment, with ER levels decreasing during therapy and rising with disease progression, making [^{18}F]FES a valuable tool for monitoring ER dynamics [100]. To optimize patient selection for anti-estrogenic therapy, He et al. identified the ΔSUV_{max} (changes in SUV_{max}) $\geq$38.0% after four weeks as the most accurate predictor of therapy response, outperforming both baseline and 4-week SUV_{max} [101]. A study by You et al. in metastasis ER-positive patients receiving aromatase inhibitors showed that [^{18}F]FES can detect ER changes in a timely manner, including ER-negative conversion, enabling early switches to chemotherapy and potentially improving survival outcomes. This was especially evident in primary tumors with low ER, where around 70% of metastatic tumors showed [^{18}F]FES negativity [102].

The tracer enables the detection of ER changes as early as 7 days following anti-estrogen therapy with or without docetaxel, as demonstrated by Liu et al. in preclinical models. When combined with [^{18}F]FDG, [^{18}F]FES provides valuable information on the decrease in ER expression as an indicator of docetaxel responsiveness following combined therapy [103]. A study by Gennari et al. found that a baseline SUV_{max} cut-off < 2 helps identify endocrine-resistant patients who benefit more from chemotherapy, showing longer progressive-free survival (PFS) with chemotherapy (23 months) compared to endocrine therapy (12.4 months) [104].

In progressive ER-positive patients previously eligible for endocrine therapy, treatment with vorinostat (an HDAC inhibitor) combined with an aromatase inhibitor showed >6 months without progression in 4/10 patients (n = 10) who stuck with the protocol, possibly due to vorinostat's ability to restore ER sensitivity. Baseline [^{18}F]FES imaging predicted response in FES-positive individuals, although no changes in tracer uptake were observed after vorinostat therapy, as shown by Peterson et al. [105]. In another study by Liu et al. involving ER-positive patients starting palbociclib in combination with endocrine therapy, [^{18}F]FES successfully predicted treatment response, with significantly longer PFS seen in

FES-positive patients (23.6 months vs. 2.4 months) and in those with a low heterogeneity index (HI) [106].

Another alternative tracer targeting the ERα receptor in breast tumors is 4-Fluoro-11β-methoxy-16α-[^{18}F]fluoroestradiol ([^{18}F]4FMFES). In a preclinical study by Paquette et al. involving ER-positive and ER-knockdown tumors, [^{18}F]4FMFES was able to differentiate between positive and negative ER tumors and demonstrated significantly higher tumor uptake and TBR compared to [^{18}F]FES. However, it also shows notable increased uptake in the uterus and ovaries. ER specificity was confirmed by a marked reduction in tumor uptake following fulvestrant administration [107]. Despite its higher abdominal uptake compared to [^{18}F]FES, this can be mitigated using loperamide and anticholinergic agents, which enhance tumor contrast by reducing abdominal uptake [108]. In a clinical study by Paquette et al. involving ER+ patients, [^{18}F]4FMFES was proven to be more stable and could detect more lesions, while organ uptake was significantly lower, including a reduction in blood uptake by 75%. However, the primary elimination route remained the gastrointestinal tract and liver, leading to persistently high liver uptake [109]. Other notable SPECT tracers that hold great potential for ER assessment, including [^{131}I]IPBA-EE [110] and [^{131}I]EITE [111], are currently under preclinical investigation.

2.3. Progesterone Receptor Imaging

There are two Progesterone receptor (PR) isoforms, PRα and PRβ. Progesterone is known to influence early events in breast carcinogenesis, with its effect on proliferation mainly via PRβ [112]. However, PRα also plays an important role in the effectiveness of anti-progesterone agents contributing to poor prognosis in anti-estrogen therapy [112,113]. Although there is no routine tool to differentiate the two isoforms, both play significant roles in breast cancer progression. PR-negative luminal cancer represents more than 10% of luminal cancer [114] and has been associated with worse outcomes [115,116]; adding chemotherapy can improve the prognosis for these PR-negative luminal cancer patients [116]. Additionally, as PR expression increases under estrogen's effect during endocrine therapy, it can serve as an indirect marker to predict and monitor therapy response by tracking receptor expression throughout treatment [117].

[^{18}F]FFNP is a tracer that targets the PR for imaging. In breast cancer patients, Dehdashti et al. have shown that the tumor-to-non-tumor uptake ratio of [^{18}F]FFNP can effectively differentiate PR positivity, with uptake ratios correlating to PR status [118]. However, similar to estrogen receptor tracers, the liver and gastrointestinal tract show high activity of [^{18}F]FFNP, which may impede lesion detection in these areas [118]. Nevertheless, Chan et al. demonstrated on preclinical models of breast cancer that [^{18}F]FFNP could detect tumor's hormone receptor changes more sensitively and earlier (day 4) than [^{18}F]FES or FDG. This allows earlier monitoring of ERα expression following estrogen deprivation therapy through a decrease in PR expression corresponding to decreased tumor uptake [119]. Conversely, low-dose estradiol-induced an increase in PR, which was trackable using [^{18}F]FFNP in a preclinical study by Salem et al. In the same study, although the tracer could not differentiate between PRα and PRβ isoforms, it significantly distinguished PR-positive from PR-negative tumors [117].

ESR1 mutations can lead to resistance to hormone therapy. A study by Kumar et al. in preclinical models of PR-positive breast cancer xenografts, with and without ESR1 mutations, demonstrated that [^{18}F]FFNP could effectively detect a decrease in tracer uptake in wild-type tumors after 7 days of endocrine therapy, while no decrease was observed in ESR1-mutant tumors, indicating therapy resistance [120]. These findings suggest that [^{18}F]FFNP may aid in the early detection of therapy resistance induced by ESR1 mutations. Furthermore, [^{18}F]FFNP was evaluated clinically by Dehdashti et al. for tracking PR changes in response to estradiol challenges in postmenopausal patients with advanced ER-positive breast cancer. The study found that post-challenge increases in tumor uptake could identify responders to endocrine therapy that the baseline scan could not. Patients with an increase in SUV_{max} > 7 were associated with significantly longer survival [121].

Several other promising candidates for progesterone receptor (PR) PET tracers are worth noting. In mouse models, Wu et al. showed [^{18}F]EAEF could differentiate between PR-positive and PR-negative breast cancer tumors with high specificity (confirmed through blocking studies in vivo). However, its biodistribution shows significant accumulation in adipose tissue due to its lipophilicity, along with high uptake in the liver and gallbladder [122]. Another preclinical study by Lee et al. explored [^{18}F]FPTP, a non-steroidal compound resistant to dehydrogenase activity, resulting in decreased liver uptake. Moreover, [^{18}F]FPTP offers several advantages over [^{18}F]FFNP, including lower bone uptake, suggesting better in vivo stability. Unlike [^{18}F]FFNP, which also binds to the glucocorticoid receptor, limiting its specificity, [^{18}F]FPTP is more selective. However, the production of [^{18}F]FPTP is limited by the presence of enantiomeric byproducts, affecting its purity [123]. Another promising candidate, [^{18}F]FPTT, demonstrated good specificity in a preclinical study by Gao et al., showing significantly higher uptake in PR-positive tumors compared to PR-negative ones, with its specificity validated by a blocking study in vivo and an increased tumor uptake following estradiol stimulation. The results highlight the tracer's improved hydrophilicity, good stability, and moderate affinity [124]. Allott et al. demonstrated that a benzoxazinthione derivative of tanaproget labeled with ^{18}F shows promising specificity in non-tumor-bearing preclinical models. However, it faces challenges due to rapid in vivo defluorination, requiring further optimization to improve stability [125].

2.4. Molecular Imaging of Ki67 Protein

Ki67 protein is active during the G1, S, G2, and M phases of the cell cycle but is not expressed in G0, anaphase, or telophase [126,127]. This makes Ki67 a key proliferation marker, particularly useful for differentiating HER2-negative luminal subtypes [3]. In the breast cancer population, the Ki67 index is approximately 25% [128], with higher levels generally associated with poor prognosis, higher metastasis rates, and increased recurrence [127,129]. High Ki67 expression varies across subtypes: it is lowest in Luminal A, followed by HER2 and TNBC, and is most frequent in Luminal B [129]. Assessing Ki67 in vivo can aid in more precise classification of breast cancer patients for optimal therapy, as Ki67 levels can predict response to systemic chemotherapy and their changes can be used to monitor therapy response [127].

Direct tracers targeting Ki-67 are not yet available. The most commonly used tracers to investigate proliferation are [^{18}F]FDG and [^{18}F]FLT. Some studies have shown a moderate correlation between FDG uptake and Ki-67 expression in lymphoma [130] and meningioma [131]. A meta-analysis by Deng et al. reported an overall correlation coefficient of $r = 0.44$ across various cancers and a similar correlation ($r = 0.44$) specifically in breast cancer [132].

Mixed results were seen when investigating the correlation between FLT and ki67 in various types of cancer (glioma, head and neck squamous carcinoma, and colorectal cancer) [133–135]. However, a meta-analysis by Chalkidou et al. revealed a strong overall correlation between FLT uptake and Ki-67 ($r = 0.7$), with particularly strong correlations observed in lung, brain, and breast cancers [136]. Further analysis by Surov et al. comparing these two tracers specifically in breast cancer found that FLT had a higher correlation with Ki-67 ($r = 0.54$) compared to FDG ($r = 0.4$) [137]. Based on this research, FLT appears to be a more relevant tracer for indirectly assessing Ki-67 levels. This is reasonable, as FLT reflects the activity of thymidine kinase, a crucial enzyme in the proliferation process [138].

A novel tracer, [^{18}F]ISO-1, has been developed by McDonald et al. as a proliferation marker targeting the σ2 receptor. The study using this tracer found a moderate correlation between [^{18}F]ISO-1 SUV_{max} and Ki-67 levels ($r = 0.46$) in invasive breast cancer patients [139].

Table 1. Summary of radiopharmaceuticals assessing conventional biomarkers in breast cancer across preclinical and clinical studies.

Imaging Biomarker	Radiopharmaceuticals		Clinical/ Preclinical Phase	Key Features	References
HER2	Trastuzumab labeled ^{89}Zr	[^{89}Zr]Zr-DFO-trastuzumab	Clinical	Effective in detecting HER2+ metastases, including brain lesions Helped predict and follow up therapy response, especially when combined with FDG PET/CT Challenges include false positives in liver and bone possibly due to instability	[29–38]
		[^{89}Zr]Zr-HOPO-trastuzumab	Preclinical	Improved stability but lower tumor uptake compared to [^{89}Zr]Zr-DFO-trastuzumab	[39]
		[^{89}Zr]Zr-DFO*-trastuzumab	Preclinical	Improved stability, retained high tumor contrast compared to [^{89}Zr]Zr-DFO-trastuzumab, and was able to visualize HER2+ metastasis in bone	[40]
		[^{89}Zr]Zr-DFO-^{ss}trastuzumab-EndoS, [^{89}Zr]Zr-DFO-^{nss}trastuzumab-PNGaseF	Preclinical	Higher tumor uptake and higher tumor contrast (especially against liver and spleen) compared to [^{89}Zr]Zr-DFO-trastuzumab Required enzymatic deglycolysating step	[41]
	Trastuzumab labeled ^{64}Cu	[^{64}Cu]Cu-DOTA-trastuzumab	Clinical	Successful for imaging HER2+ metastasis, including brain metastases Potential in predicting therapy responsesNoted transchelation with serum compounds	[43–46]
		[^{64}Cu]Cu-NOTA-trastuzumab	Clinical	Higher tumor contrast and lower off-target uptake and absorbed compared to [^{64}Cu]Cu-DOTA-trastuzumab	[47,48]
	Trastuzumab labeled ^{52}Mn	[^{52}Mn]Mn-BPPA-trastuzumab	Preclinical	Higher HER2+ tumor contrast than control [^{52}Mn]Mn-DOTAGA-trastuzumab, allowed earlier differentiating of tumor HER2 positivity Needed stability improvement	[51]
		[^{52}Mn]Mn-Oxo-DO3A-trastuzumab	Preclinical	Comparable tumor contrast to [^{52}Mn]Mn-BPPA-trastuzumab and good stability	[52]
	Pertuzumab labeled ^{89}Zr	[^{89}Zr]Zr-DFO-pertuzumab	Clinical	Was able to detect HER2+ metastasis, including brain metastasis Showed potential in predicting and follow-up therapy responses (even during trastuzumab treatment) Has slightly higher absorbed dose compared to [^{89}Zr]Zr-DFO-trastuzumab	[53–57]
		[^{89}Zr]Zr-^{ss}DFO-pertuzumab	Clinical	Improved tumor-to-liver and -spleen ratios, but increased renal absorbed dose compared to [^{89}Zr]Zr-DFO-pertuzumab	[58,59]

Table 1. *Cont.*

Imaging Biomarker	Radiopharmaceuticals		Clinical/ Preclinical Phase	Key Features	References
HER2	Trastuzumab emtansine labeled ^{89}Zr	[^{89}Zr]Zr-DFO-T-DM1	Preclinical	Higher HER2+ tumor uptake than [^{89}Zr]Zr-DFO-trastuzumab Potential in predicting T-DM1 responses	[60,61]
	Labeled trastuzumab fragments	[^{68}Ga]Ga-NOTA-F(ab')-trastuzumab, [^{68}Ga]Ga-NOTA-F(ab')$_2$-trastuzumab	Preclinical	Faster clearance than trastuzumab while retain affinity F(ab') tracer showed faster clearance and higher tumor-to-background ratios than F(ab')$_2$, except for tumor-to-kidney ratios	[62]
		[^{64}Cu]Cu-MANOTA-Fab-trastuzumab	Preclinical	Better stability and tumor contrast than using other chelators (DOTA, DOTAGA, NODAGA) Clear visualization of the HER2+ tumor from 4h p.i.	[63]
		[^{68}Ga]Ga-DFO-M74 trastuzumab's Fab	Preclinical	Better stability and higher tumor contrast compared to non-specific wild type Fab tracer	[64]
		[^{89}Zr]·DFO-HER2-Fab-PAS$_{200}$	Clinical	Extended biological half-life and improved tumor visualization including metastasis	[65,66]
	HER2 nanobody	[^{18}F]TFPFN-5F7, [^{18}F]TFPFN-2Rs15d	Preclinical	Lower kidney uptake, improved tumor contrast compared to tracers using other ^{18}F prosthetics	[67]
		[^{68}Ga]Ga-NOTA-2Rs15d	Clinical	Confirmed safety and reproducibility, able to detect inter-lesion heterogeneityDiscordance with IHC results posed challenges	[68,69]
		[^{89}Zr]Zr-DFO-2Rs15d	Preclinical	Explored the biodistribution of the tracer at later time points, kidney uptake remained a dosimetry challenge	[70]
		[^{68}Ga]Ga-ABY-025	Clinical	Detected HER2 heterogeneity and was able to follow HER2 targeting therapyTumor uptake correlation with IHC was not significant	[74–78]
	HER2 affibody	[^{18}F]F-Al-MAL-NOTA-Cys-MZHER$_{2:342}$	Preclinical	Good HER2 specificity with lower liver uptake than ZHER$_{2:342}$ tracers. Low bone uptake indicated tracer stability	[79]
		[^{68}Ga]Ga-MAL-NOTA-Cys-MZHER$_{2:342}$	Clinical	Able to differentiate HER2 positivityLower liver uptake compared to ABY-025 tracer	[80]
		[^{89}Zr]Zr-DFO-MAL-NOTA-Cys-MZHER$_{2:342}$	Preclinical	Good HER2 specificity with low liver and bone uptake; indirectly indicated tracer's stability	[81]

Table 1. *Cont.*

Imaging Biomarker	Radiopharmaceuticals		Clinical/ Preclinical Phase	Key Features	References
HER2	Other HER2 scaffolds and peptides	[^{89}Zr]Zr-DFO-G3-DARPin	Preclinical	High HER2 affinity and specificity but prominent kidney uptake and slow site-specific conjugation step	[85]
		[^{68}Ga]Ga-DOTA-(Ser)$_3$-LTVSPWY	Preclinical	Good HER2+ tumor visualization, and tracer's stability despite prominent kidney uptake	[89]
		[^{68}Ga]Ga-DOTA-PEG$_2$-DTFPYLGWWNPNEYRY, [^{68}Ga]Ga-DOTA-PEG$_2$-GSGKCCYSL	Preclinical	[^{68}Ga]Ga-DOTA-PEG$_2$-DTFPYLGWWNPNEYRY showed better human serum stability and more significant differentiation of HER2-positivty 1h p.i. than [^{68}Ga]Ga-DOTA-PEG$_2$-GSGKCCYSL	[90]
Estrogen Receptor Alpha		[^{18}F]FES	Clinical	Improved metastasis detection in ER-positive patients when combined with FDG, especially in bone lesions Could predict and follow ER changes during endocrine therapy	[97–106]
		[^{18}F]4FMFES	Clinical	Improved tumor contrast and lower organ uptake compared to [^{18}F]FES, but high uterus and ovary uptake in preclinical models	[107,109]
Progesterone Receptor		[^{18}F]FFNP	Clinical	Differentiated PR-positive tumors; predicted hormone therapy responses and early detection of both PR and ER changes during the therapy Challenges include high uptake in liver and gastrointestinal tract	[117–121]
		[^{18}F]EAEF	Preclinical	Differentiated tumor PR positivity, high adipose and abdominal uptake due to lipophilicity	[122]
		[^{18}F]FPTP	Preclinical	Greater PR selectivity and lower liver uptake compared to [^{18}F]FFNP; reduced bone uptake indicated in vivo stabilityEnantiomeric byproducts may impair purity	[123]
		[^{18}F]FPTT	Preclinical	Improved hydrophilicity and stability; effectively distinguishes PR-positive tumors with significant specificity	[124]
Ki67		[^{18}F]FDG	Clinical	Correlation with Ki67 expression in breast cancer is moderate (r = 0.4)	[132,137]
		[^{18}F]FLT	Clinical	Stronger correlation with Ki67 in breast cancer (r = 0.54)	[136,137]
		[^{18}F]ISO-1	Clinical	Moderate correlation with Ki67 in invasive breast cancer (r = 0.46)	[139]

3. Novel Imaging Biomarkers

3.1. Epidermal Growth Factor Receptor Imaging

EGFR belongs to a family of transmembrane glycoproteins with similar structures and signaling pathways, whose interactions significantly influence cancer cell activity [140]. EGFR overexpression is observed in at least 15% of breast cancers [141]. Although expressed across all subtypes, EGFR is most commonly found in aggressive forms, particularly TNBC (around half of the cases) [140,142]. High EGFR expression generally correlates with poor outcomes, especially in TNBC, and is associated with higher metastasis rates. In contrast, in luminal subtypes, EGFR expression has been linked to improved survival [142]. Among HER2-enriched breast cancer population, the close interplay between EGFR and HER2 receptors also contributes to poor prognosis, as patients with co-expression of these proteins often exhibit therapy resistance [143]. Therefore, proper EGFR imaging can be a promising tool for selecting candidates for EGFR targeting therapy, potentially improving prognosis, especially in aggressive subtypes.

A study by Sadri et al. using [^{64}Cu]Cu-DOTA-cetuximab on breast cancer xenografts with high levels of EGFR demonstrated efficient tumor specificity (confirmed with a blocking study in vivo), achieving a tumor-to-blood ratio of approximately 2 (2 h post-injection). Notably, after extended blocking (24 h blocking) with unlabeled cetuximab, the tumor exhibited increased tracer uptake, potentially due to the regeneration of EGFRs on the cell surface [144]. With the same antibody, a study by McKnight et al. using [^{89}Zr]Zr-DFO-cetuximab on TNBC breast cancer xenografts with varying EGFR levels, the tracer effectively stratified EGFR expression. The tracer also showcased its potential in tracking dynamic changes in EGFR expression. Specifically, the increase in membranous EGFR under dasatinib treatment, which indirectly indicates the regaining of sensitization to cetuximab, strongly correlated ($r > 0.8$) with the increased tumor uptakes [145].

Similarly, Bhattacharyya et al., using [^{89}Zr]Zr-DFO-panitumumab, demonstrated a strong correlation ($r^2 = 0.857$) between tumor uptake and EGFR expression in mice carrying breast cancer xenografts, with notably elevated lymph node activity [146]. In a preclinical study by Cavaliere et al. on TNBC xenografts, [^{89}Zr]Zr-DFO-amivantamab (a bispecific antibody against EGFR and cMET) demonstrated dual specificity, highlighting its potential for selecting candidates for amivantamab therapy [147].

Another study by Tikum et al., in preclinical models carrying colorectal and breast cancer, used [^{89}Zr]Zr-DFO-matuzumab, targeting a different EGFR epitope compared to nimotuzumab, and showed high specificity for EGFR. The tracer's uptake was significantly blocked by unlabeled matuzumab but not by nimotuzumab. Additionally, the tracer successfully visualized tumors regardless of KRAS mutation status, a factor known to induce anti-EGFR resistance and that can decrease tumor uptake [148]. In a separate study by Chekol et al., [^{89}Zr]Zr-DFO-nimotuzumab effectively differentiated EGFR-positive from EGFR-negative breast cancer xenografts starting at 24 h post-injection, with the greatest distinction observed at 7 days post-injection. This tracer also demonstrated a lower absorbed dose compared to [^{89}Zr]Zr-DFO-trastuzumab [149].

Further research by Solomon et al. used site-specific labeling with SpyTag/SpyCatcher to produce [^{89}Zr]Zr-DFO-nimotuzumab- SpyTag-ΔN-SpyCatcher. The tracer could visually differentiate EGFR-positive and -negative tumors in preclinical models, with high specificity for EGFR (a marked decrease in positive tumor uptake when imaging with [^{89}Zr]Zr-control-IgG-SpyTag-ΔN-SpyCatcher). Additionally, [^{255}Ac]Ac-nimotuzumab labeled using this method showed higher survival rates compared to the unlabeled antibody, suggesting its potential for radioimmunotherapy [150].

Another preclinical study in breast cancer, colorectal, and melanoma tumors by Alizadeh et al. used an EGFR domain II-specific antibody fragment, 8709, labeled with ^{89}Zr. This fragment, targeting a different domain than nimotuzumab, demonstrated good specificity. Tumor uptake was significantly blocked by unlabeled scFc-Fc, but not by nimotuzumab, and could distinguish EGFR positivity as early as day 2. However, as expected with small antibody fragments, kidney uptake remained the highest [151]. Recently, an

EGFR affibody labeled with ^{89}Zr using a novel cyclic fusarinine C chelator ([^{89}Zr]Zr-FSC-ZEGFR:2377) was studied by Summer et al. in mice with epidermoid carcinoma xenografts, yielding favorable results both in vitro and in vivo [152].

3.2. Human Epidermal Growth Factor Receptor 3 Imaging

Human epidermal growth factor receptor 3 (HER3), also a member of the EGFR/ERBB family of receptor tyrosine kinases, plays a crucial role in cancer progression by activating the PI3K-AKT-mTOR pathway upon heterodimerization with other receptors [153]. Among the breast cancer population, HER3 overexpression was found in at least more than 18% of the cases [154]. It is especially associated with the HER2 subtype, showing a tendency for brain metastasis, which reduces survival rates and contributes to resistance against HER2-targeted therapies [155]. Additionally, HER3 overexpression worsens prognosis in TNBC, particularly when co-expressed with EGFR [156]. As a result, HER3-targeting therapies, such as lumretuzumab and patritumab, have been actively studied, showing promising efficacy and tolerable side effects [154]. Early in vivo HER3 imaging may enhance the prediction of response to HER3-targeted therapies in breast cancer, supporting more personalized treatment approaches.

Several studies have investigated the use of [^{89}Zr]-labeled antibodies for imaging breast cancer in preclinical and clinical settings. Bensch et al. utilized [^{89}Zr]Zr-DFO-lumretuzumab to target HER3 in patients with advanced cancers, including breast cancer. It was found that the optimal tumor-to-background contrast was achieved with a dose of 100 mg of unlabeled lumretuzumab and with imaging performed 4 or 7 days post-injection. This approach successfully visualized 67.6% of lesions $\geq$ 10 mm detected by CT, including some brain lesions and previously undetected bone metastases. However, the detection of lung and liver lesions was less reliable, and uptake did not correlate with HER3 expression as determined by IHC [157]. In a separate clinical study (n = 6) by Oordt et al. using [^{89}Zr]Zr-DFO-GSK2849330, another HER3-targeting antibody, it was observed that an 8 mg dose provided the best tumor contrast on day 5 post-injection. This study also noted that tumor uptake was saturable at a dose of 30 mg/kg, demonstrating the tracer's specificity for targeting HER3. The tracer successfully visualized and quantified lesions in bones, soft tissues, and lungs. Nonetheless, there was no correlation between lesion uptake and the treatment response to the antibody [158].

Imaging with HER3 antibodies to assess therapy effects has been conducted in breast cancer-bearing mice. In one study by Pool et al., [^{89}Zr]Zr-DFO-mAb3481 was used during lapatinib therapy. This tracer achieved tumor-to-blood ratios exceeding 50—higher than those observed in other studies using HER3 affibodies, which have the advantages of high affinity and rapid clearance for high tumor contrast. The study found no changes in tumor uptake, which was consistent with the stable HER3 expression in xenografts during treatment as confirmed by IHC, thus validating the tracer's accurate HER3 expression assessment [159].

Antibody fragments targeting HER3 show great promise for assessing HER3 status in breast cancer preclinical models. For instance, [^{64}Cu]Cu-CB-TE2A-F(ab')2-mAb105 was used by Wehrenberg-Klee et al. to monitor cellular changes under AKT and PI3K inhibitors, demonstrating a significant relationship between tumor uptake and increased HER3 levels after therapy. This tracer also effectively detected the treatment-induced increase in receptor tyrosine kinase levels [160].

HER3 affibodies offer a significantly higher tumor contrast than antibodies or antibody fragments, as shown by compaing ZHER$_{3:08698}$ with seribantumab and its fragments [161]. A study by Rosestedt et al. using [^{68}Ga]Ga-HEHEHE-ZHER$_{3:8698}$-NOTA in preclinical models with various cancers, including breast cancer, demonstrated the tracer's high specificity for HER3, showing a significant correlation (r = 0.66) between tumor uptake and HER3 expression. The tracer exhibited significantly higher uptake in HER3-positive breast cancer xenografts compared to HER3-negative tumors and could become saturated with an excess dose of the affibody [162]. Another study by Da Pieve et al. compared [^{18}F]AlF-NOTA-

$ZHER_{3:8698}$ with [^{18}F]AlF-NODA-$ZHER_{3:8698}$ in breast cancer mouse models, revealing that both tracers visualized the tumors 1 h post-injection. However, the NOTA-conjugated tracer provided better TBRs, though its chelation process requires high temperatures, which can be challenging for heat-sensitive peptides [163]. HER3 affibody tracers can also be used to evaluate therapy resistance, as the activation of the HER3 pathway is one of the mechanisms responsible for resistance to anti-HER2 therapy. In a preclinical model by Martins et al., the HER3-specific tracer [^{89}Zr]Zr-DFO-$ZHER_{3:8698}$ demonstrated high specificity for HER3, effectively stratifying HER3 expression in correlation with IHC staining. This tracer was used to assess changes in HER3 uptake following HSP90 inhibitor treatment. Two weeks after initiating treatment, tumor uptake of the tracer significantly increased, corresponding to elevated HER3 expression [164]. In another preclinical study by Wehrenberg-Klee et al., the peptide-based tracer [^{68}Ga]Ga-NOTA-ßAGGG-CLPTKFRSC effectively detected changes in HER3 expression (with nearly a threefold increase in uptake) in HER2-positive lapatinib-resistant xenografts after 2 days of treatment, enabling the timely selection of a more effective treatment plan by supplementing HER3-targeting siRNA along with lapatinib [165].

3.3. Vascular Endothelial Growth Factor Imaging

According to IHC results, at least 70% of breast cancer cases are positive for VEGF [166]. VEGF expression is most frequently associated with HER2-positive subtypes, followed by Luminal B and TNBC, and is least common in Luminal A subtypes [166,167]. VEGF, particularly VEGF-A, is crucial for the angiogenesis required for tumor growth, with VEGF receptors such as VEGFR1 and VEGFR2, which have a high affinity for VEGF-A, playing vital roles in breast cancer progression [168]. While recent therapies targeting VEGF-A or VEGFR2 [169,170] have shown mixed results, new anti-angiogenic agents are currently being explored in breast cancer treatment [171]. Thus, assessing VEGF and VEGFR expression in vivo may aid in selecting patients who are suitable candidates for these therapies.

Imaging VEGF with [^{89}Zr]Zr-DFO-bevacizumab has been studied in breast cancer patients by Gaykema et al., showing clear tumor visualization with good contrast 4 days post-injection. Tumor uptake was significantly higher than for normal breast tissue, and SUV_{max} correlated with VEGF IHC (r = 0.49). Interestingly, increased uptake in the nipples was noted, likely due to elevated perfusion in these areas [172]. In a preclinical TNBC xenograft study by Scheltinga et al., the same tracer visualized a decrease in VEGF expression following HSP90 inhibitor treatment compared to the baseline uptake [173]. However, a clinical study by Gaykema et al. demonstrated that only the tumor uptake of [^{89}Zr]Zr-DFO-trastuzumab, and not of [^{89}Zr]Zr-DFO-bevacizumab, correlated with tumor size changes following HSP90 inhibitor treatment, as assessed by CT imaging [37].

A recent preclinical study by Yang et al. used [^{89}Zr]Zr-DFO-aflibercept (Abe), a fusion protein targeting VEGF-A, VEGF-B, and placental growth factor (PlGF), to visualize TNBC xenografts. The tracer demonstrated high tumor contrast with confirmed specificity; however, it also showed high uptake in the liver, identifying the liver as the critical organ [174].

VEGF peptides labeled with PET isotopes have also been used for imaging VEGFR in TNBC breast tumor-bearing mice, especially VEGFR2, which is the crucial target in antiangiogenic therapy. In contrast, VEGFR1 is predominantly expressed physiologically in the kidneys. Wang et al. developed a mutated recombinant form of $VEGF_{121}$, known as $VEGF_{DEE}$, labeled with ^{64}Cu via a DOTA chelator to selectively target VEGFR2. This tracer demonstrated slightly higher tumor uptake and reduced kidney uptake at all time points compared to [^{64}Cu]Cu-DOTA-$VEGF_{121}$. Nevertheless, both tracers showed strong tumor specificity, with uptake significantly blocked by the addition of unlabeled peptides in vivo [175]. Another tracer developed by Zhang et al., [^{61}Cu]Cu-NOTA-K3-$VEGF_{121}$, which features 3 lysine modification at the N-terminus for easier labeling, also demonstrated

good specificity in a blocking study in vivo using an unlabeled compound, although the liver, gastrointestinal tract, and kidney showed remarkable activity [176]. In another study by Meyer et al., [^{89}Zr]Zr-DFO-labeled single-chain VEGF-A mutants targeting VEGFR1 and VEGFR2 were compared with pan-receptor-selective scVEGF in TNBC-bearing mice. All compounds successfully visualized tumors at 2 h post-injection, with specificity validated by blocking studies in vivo with corresponding unlabeled peptides. However, kidney uptake was prominent, particularly with scVEGF-R1, due to physiological VEGFR expression [177].

In addition to renal VEGFR1 expression, many conditions involving neovascularization, such as atherosclerosis, stroke, and osteoarthritis, can provide a false positive when imaging tumor VEGFR, especially in the brain and bones, which are frequent sites of breast cancer metastasis. In fact, molecular imaging targeting these receptors has been used to visualize plaque [178] and post-stroke neoangiogenesis [179].

3.4. Androgen Receptor Imaging

The androgen receptor (AR) is expressed in over 70% of breast cancer cases, with positivity most prevalent in luminal subtypes, followed by TNBC [180]. In luminal subtypes, AR positivity has a notable impact on prognosis, as patients who are positive for both androgen and estrogen receptors generally experience better outcomes than those who are AR-negative [181]. Furthermore, in the TNBC subtype, AR positivity is observed in more than half of cases [182] and is associated with improved prognosis, suggesting that these patients may benefit from anti-androgen therapies [182,183]. Given the significant role of AR in breast cancer prognosis and treatment response, effective imaging to assess AR expression could greatly enhance patient selection for anti-androgen therapies, leading to more personalized and potentially more effective treatment strategies.

[^{18}F]FDHT has been employed for androgen receptor (AR) imaging, with a study by Venema et al. in postmenopausal hormone receptor-positive breast cancer patients showing the tracer's ability to visualize tumors with a sensitivity of 91% and a specificity of 100%. The tracer's SUV_{max} was found to correlate moderately (r^2 = 0.47) with AR IHC [184]. In a longitudinal study by Boers et al. in postmenopausal patients with AR-positive metastatic breast cancer receiving bicalutamide therapy, [^{18}F]FDHT was able to track reductions in tumor uptake 4–6 weeks following treatment, but these reductions did not correlate consistently with therapy responses. Notably, significantly greater reductions were observed in ER-negative patients [185]. Another study by Jacene et al. involving serial imaging in estrogen receptor-positive postmenopausal patients undergoing selective AR modulation (SARM) therapy with GTx-024 demonstrated a greater reduction in tumor uptake in patients experiencing clinical benefit, although the difference was not statistically significant and the sample size was limited (n = 11) [186]. Recently, [^{18}F]enzalutamide was evaluated in prostate cancer xenografts, demonstrating high specificity and stability as an AR-targeted tracer, suggesting that [^{18}F]enzalutamide could potentially be adapted for imaging androgen receptors in breast cancer [187].

3.5. Estrogen Receptor Beta Imaging

Estrogen receptor beta (ERβ) is physiologically expressed in various organs, including the ovaries, central nervous system, male reproductive organs, colon, kidneys, and immune system [188]. Estrogen beta plays a protective role in breast cancer. Its expression levels are significantly lower in breast cancer tissues compared to healthy breast tissue, especially in higher-grade tumors [189]. ERβ positivity is observed in over 68% of breast cancer cases, with the highest prevalence in luminal subtypes [190], where it is generally associated with a favorable prognosis [191]. In TNBC, ERβ expression appears to be linked to better outcomes and treatment efficacy through multiple pathways [192]. However, the prognostic significance of ERβ in TNBC remains controversial due to the presence of various receptor isoforms, which may contribute to the complexity of its role in this subtype [193]. Given its

protective role and prognostic value, ERβ-targeted imaging could be crucial for predicting the effectiveness of ERβ agonists, aiding in patient selection and personalized treatment.

In efforts to develop an ERβ tracer, a study using [^{18}F]FEDPN in ERα-knockout and ERβ-knockout mice demonstrated ovary and uterus uptake mediated by ERβ. However, the tracer's specificity was moderate, as the ovary—despite being the organ with the highest ERβ expression—showed only minor uptake differences between the knockout models [194].

Other studies on ovarian and prostate xenografts in preclinical models used [^{18}F]PVBO, which confirmed specificity through blocking studies [195], and [^{18}F]FHNP, where tumor uptake correlated with ERβ expression, validating its receptor selectivity [196]. Although no studies have yet been conducted in breast cancer-bearing mice, the tracers mentioned above show significant potential for assessing ERβ expression in breast cancer. Nevertheless, caution is required as there is considerable physiological expression of the receptor in organs such as the ovary and uterus.

3.6. Poly (Adenosine Diphosphate [ADP]-Ribose) Polymerase 1 Imaging

Poly (ADP-ribose) polymerase 1 (PARP1) is a crucial enzyme in the DNA repair pathway [197], making it a significant target for synthetic lethality in cancers with BRCA1 and BRCA2 mutations. PARP inhibitors have shown promise in improving survival rates for patients with these mutations [198]. Particularly, high PARP1 expression is generally associated with a poorer prognosis [199]. Although BRCA mutations often correlate with elevated PARP1 levels [199], not all BRCA-mutated cancers respond effectively to PARP inhibitors, and some non-BRCA-mutated cancers also exhibit high PARP1 expression [200]. Furthermore, PARP1 expression varies across breast cancer subtypes: HER2-positive and TNBC show higher nuclear expression, whereas luminal subtypes display increased cytoplasmic and overall expression [201,202]. The complex heterogeneity of breast cancer emphasizes the importance of assessing PARP1 expression in vivo to optimize the personalized and effective use of PARP1 inhibitors in therapy.

[^{18}F]FluorThanatrace ([^{18}F]FTT) has been used to assess PARP1 expression in preclinical studies. Zhou et al. demonstrated its specificity by visualizing TNBC tumors at 60 min post-injection, with uptake significantly decreased by an unlabeled compound or olaparib [203]. Tumor uptake correlated with PARP1 expression levels [204], and despite high abdominal uptake due to hepatobiliary clearance [203], tumor contrast was sufficient, with a tumor/muscle ratio of 1.9 observed in the group with the highest PARP1 expression [204]. In a small study by McDonald et al. (n = 4) in breast cancer patients, the tracer detected a reduction in SUV_{max} post-PARPi therapy, highlighting its potential for monitoring PARP1 expression in clinical settings [205].

Another candidate studied by Xu et al., [^{18}F]-PARPi, an [^{18}F]-labeled olaparib derivative, showed high specificity in TNBC xenografts, with tumors visualized 1 h post-injection, and blocking studies with olaparib reduced tumor uptake. Additionally, the block study also decreased spleen and pancreas uptake, explaining the elevated abdominal uptake observed in PARP1 imaging studies [206]. In a comparative study by Stotz et al. in breast cancer-bearing mice, their novel [^{18}F]FPyPARP showed the highest tumor-to-blood ratios, while [^{18}F]-PARPi had the highest tumor-to-muscle and tumor-to-kidney contrast, and [^{18}F]FTT exhibited the highest tumor uptake and longer retention [207].

[^{18}F]Talazoparib, the most potent PARPi labeled with ^{18}F, was evaluated by Bowden et al. in breast cancer models, showing high specificity and significant tumor blocking by talazoparib and olaparib in vitro. The tracer also demonstrated exceptionally high tumor-to-blood ratios (around 10), outperforming [^{18}F]FTT and [^{18}F]-PARPi, with similar hepatic and renal clearance, though its enantiomer complicates tracer production [208].

Other potential PARP1-targeting tracers have been tested in preclinical models carrying breast cancer. Shuhendler et al. used [^{18}F]SuPAR to monitor PARP1 levels with high specificity, evidenced by a significant reduction in tumor uptake when treated with talazoparib. There were increases in tumor uptake in a dose- and time-dependent manner following radiotherapy, which activates PARP1 in the similar manner [209]. Zheng et al. developed [^{18}F]BIBD-300, a tracer with reduced lipophilicity favoring renal clearance, and evaluated it in breast cancer-bearing mice. Although [^{18}F]BIBD-300 showed lower tumor uptake compared to [^{18}F]FTT, it provided superior tumor contrast, with significantly higher tumor-to-muscle and tumor-to-liver ratios [210].

3.7. Programmed Death-Ligand 1 Imaging

Most breast cancers have some degree of tumor-infiltrating lymphocytes (TILs), with approximately 10% showing more than 50% lymphocytic infiltration. This group of predominant TIL tumors is generally associated with better outcomes in breast cancer patients and often shows elevated expression of PD-L1 [211]. Notably, there is a correlation between PR ER negativity and high PD-L1 expression. Consequently, HER2-enriched and TNBC subtypes both show particularly high PD-L1 levels, particularly in TNBC, despite these subtypes' aggressive nature [212]. Given this, immune checkpoint inhibitor therapy in breast cancer can be more beneficial in treating TNBC [211]. However, the response rate in metastatic TNBC has been moderate, with a PFS of 2 months and an overall survival (OS) of 8.8 months, even in the PD-L1-positive patients [213]. The prognosis can be improved when combined with chemotherapy, especially in cancer with high PD-L1 expression, i.e., the PFS for the combined group was significantly longer than for the chemotherapy group, (with a hazard ratio of 0.69, even though the OS was not significantly different) [214]. Therefore, a noninvasive, in vivo assessment of PD-L1 status could be a valuable tool for selecting patients who would benefit from immune checkpoint inhibitor therapy.

In preclinical TNBC models, Massicano et al. utilized [^{89}Zr]Zr-DFO-atezolizumab to image PD-L1 expression. The tracer effectively visualized tumors 7 days post-injection, with specificity confirmed through both in vitro and in vivo blocking studies. However, substantial uptake in the spleen, liver, kidneys, and adrenal glands led to high absorbed doses in these organs and limited tumor contrast. The study further demonstrated elevated tracer tumor contrast following treatment with niraparib (a PARP inhibitor) or chemotherapy; both upregulate PD-L1 expression [215]. In a clinical study by Bensch et al. involving patients with various cancer types, including TNBC, imaging performed at 4 and 7 days post-injection (preceded with 10 mg of unlabeled atezolizumab) revealed significant tracer accumulation in the liver, spleen, bone marrow, and lymphoid tissues. Notably, higher tumor SUV_{max} on PET images was more strongly correlated with positive responses to PD-L1 therapy than PD-L1 IHC results [216].

In preclinical TNBC models, Jagoda et al. demonstrated that [^{89}Zr]Zr-DFO-avelumab exhibited a similar biodistribution, with high radioactivity levels in the spleen, lymph nodes, liver, bone marrow, and moderate uptake in tumors. Blocking studies using escalating doses (10 μg up to 400 μg) of unlabeled avelumab showed decreased spleen and liver uptake, with increased tumor and lymph node uptake at lower doses [217]. In a separate study by Li et al., pre-blocking with 1.5 mg of cold avelumab similarly reduced uptake in both the tumor and spleen, while liver uptake increased, suggesting strong non-tumor-specific binding in the spleen [218].

Table 2. Summary of radiopharmaceuticals assessing novel biomarkers in breast cancer across preclinical and clinical studies.

Imaging Biomarker	Radiopharmaceuticals		Clinical/ Preclinical Phase	Key Features	References
EGFR	Labeled antibody	[^{64}Cu]Cu-DOTA-cetuximab	Preclinical	Efficient tumor specificity in EGFR-expressing breast cancer; tracked the increase in EGFR after extended blocking	[144]
		[^{89}Zr]Zr-DFO-cetuximab	Preclinical	Stratifies EGFR expression in TNBC xenografts; correlated with treatment-induced receptor changes	[145]
		[^{89}Zr]Zr-DFO-panitumumab	Preclinical	Strong correlation between uptake and EGFR expression; lymph node activity observed in xenografts	[146]
		[^{89}Zr]Zr-DFO-amivantamab	Preclinical	Demonstrated dual specificity for EGFR and cMET	[147]
		[^{89}Zr]Zr-DFO-matuzumab	Preclinical	High specificity for EGFR; visualized tumors regardless of KRAS mutation status	[148]
		[^{89}Zr]Zr-DFO-nimotuzumab	Preclinical	Differentiates EGFR-positive/negative tumors; lower absorbed dose compared to [^{89}Zr]Zr-DFO-trastuzumab	[149]
		[^{89}Zr]Zr-DFO-nimotuzumab-SpyTag-ΔN-SpyCatcher	Preclinical	High specificity with reduced off-target effects; potential for theragnostic radioimmunotherapy.	[150]
	Labeled antibody fragment	[^{89}Zr]Zr-DFO-8709-scFv-Fc	Preclinical	Early to differentiate EGFR positivity (2 days p.i.) with high specificityKidney uptake was prominent	[151,157]
HER3		[^{89}Zr]Zr-DFO-lumretuzumab	Clinical	Visualizes HER3-positive tumors, including brain metastases; limited reliability in lung/liver lesions	[157]
	Labeled HER3 antibody	[^{89}Zr]Zr-DFO-GSK2849330	Clinical	Saturable uptake; visualized lesions in bones, soft tissues, and lungs; no correlation with treatment response	[158]
		[^{89}Zr]Zr-DFO-mAb3481	Preclinical	Higher tumor-to-blood ratios overserved in HER3 affibodies, following HER3 expression under therapy	[159]

Table 2. *Cont.*

Imaging Biomarker	Radiopharmaceuticals		Clinical/ Preclinical Phase	Key Features	References
HER3	Labeled antibody fragments	[^{64}Cu]Cu-CB-TE2A-F(ab')2-mAb105	Preclinical	Monitors HER3 level and level of tyrosine kinase activity changes under therapy	[160]
	HER3 affibody	[^{68}Ga]Ga-HEHEHE-ZHER$_{3:8698}$-NOTA	Preclinical	High specificity and tumor contrast with significant correlation between tumor uptake and HER3 level	[162]
		[^{18}F]AlF-NOTA-ZHER$_{3:8698}$	Preclinical	Promising HER3 visualization as early as 1h p.i.; better tumor-to-background ratio than conjugation with NODA	[163]
		[^{89}Zr]Zr-DFO-ZHER$_{3:8698}$	Preclinical	High specificity; effective for assessing HER3 expression changes under therapy	[164]
	HER3 peptide	[^{68}Ga]Ga-NOTA-ßAGGG-CLPTKFRSC	Preclinical	Effective for assessing HER3 expression changes under therapy	[165]
VEGF/VEGFR	VEGF antibody	[^{89}Zr]Zr-DFO-bevacizumab	Clinical	Visualizes VEGF-positive tumors; correlates moderately with VEGF IHC; high uptake in nipples observedPotential to follow VEGF expression changes during therapy	[37,172,173]
	VEGF antagonist	[^{89}Zr]Zr-DFO-aflibercept	Preclinical	Targets VEGF-A/B and PlGF; high tumor contrast; liver identified as critical organ	[174]
	VEGF and derivatives	[^{64}Cu]Cu-DOTA-VEGF$_{DEE}$	Preclinical	Selectively targets VEGFR2; strong tumor specificity with reduced kidney uptake compared to VEGF$_{121}$ tracer	[175]
		[^{61}Cu]Cu-NOTA-K3-VEGF$_{121}$	Preclinical	Facile labelling with good specificity but elevated liver, gastrointestinal tract, kidney uptakes	[176]
	Single-Chain VEGF Mutants	[^{89}Zr]Zr-DFO-scVR1, [^{89}Zr]Zr-DFO-scVR2	Preclinical	High specificity with the respective receptors (VEGFR1 and VEGFR2); kidney uptake was prominent	[177]
Androgen Receptor		[^{18}F]FDHT	Clinical	Visualizes AR-positive tumors; correlated moderately with AR IHC; tracks therapy-induced uptake changes	[184–186]

Table 2. *Cont.*

Imaging Biomarker	Radiopharmaceuticals	Clinical/ Preclinical Phase	Key Features	References
PARP1	[^{18}F]FTT	Clinical	Correlates with PARP1 expression; sufficient tumor contrast; high abdominal uptake noted in preclinical results Potential to track PARP1 reduction after therapy	[203–205,207]
	[^{18}F]-PARPi	Preclinical	High specificity in TNBC xenografts; reduced uptake in spleen and pancreas with blocking studies	[206,207]
	[^{18}F]FPyPARP	Preclinical	Showed the highest tumor-to-blood ratios compared to [^{18}F]FTT and [^{18}F]-PARPi	[207]
	[^{18}F]Talazoparib	Preclinical	Higher tumor-to-blood ratios than [^{18}F]FPyPARP; challenging tracer production with enantiomer	[208]
	[^{18}F]SuPAR	Preclinical	Able to track the PARP1 level changes after therapy in a dose- and time-dependent manner	[209]
	[^{18}F]BIBD-300	Preclinical	Reduced lipoplicity to improve tumor-to-liver ratios	[210]
PD-L1	PD-L1 antibody	[^{89}Zr]Zr-DFO-atezolizumab	Clinical	Able to predict and follow up therapy responses High uptake in spleen, liver, and bone marrow limited tumor contrast	[215,216]
		[^{89}Zr]Zr-DFO-avelumab	Preclinical	Effective in imaging PD-L1; biodistribution varied with pre-blocking, high specific spleen uptake	[217,218]
		[^{64}Cu]Cu-NOTA-MX001	Preclinical	Improved tumor contrast that overcame spleen liver uptakes	[219]
		[^{64}Cu]Cu-NOTA-durvalumab	Preclinical	High specificity, further bettered tumor-to-liver and -spleen ratios but increased blood pool uptake	[220]
		[^{89}Zr]Zr-p-SCN-Bn-C5HOPO-STM108	Preclinical	Superior tumor contrast compared to [^{89}Zr]Zr-DFO-STM108, with tumor uptake higher than liver and spleen uptakes	[221]

In another approach by Xu et al., [^{64}Cu]Cu-NOTA-MX001, a fully human anti-PD-L1 antibody labeled with ^{64}Cu was used in mice bearing PD-L1-positive colorectal cancer and -negative TNBC cancer. Despite initially elevated liver and spleen uptake, PD-L1-positive tumors became the highest uptake tissue by day 2 post-injection [219]. Similarly, [^{64}Cu]Cu-NOTA-durvalumab was used by Malih et al. in TNBC and pancreatic cancer xenografts, demonstrating high specificity. PD-L1-positive TNBC tumors showed approximately fivefold higher uptake than negative tumors 2 days post-injection, while significantly lower uptake was observed in positive tumors using a [^{64}Cu]Cu-NOTA-IgG control. Moreover, this tracer provided excellent tumor contrast, with the tumor exhibiting the highest uptake, followed by the blood, while liver and spleen uptake remained moderate [220]. A novel PD-L1 tracer, developed by Radaram et al., [^{89}Zr]Zr-p-SCN-Bn-C5HOPO-STM108, was tested in PD-L1-positive TNBC xenografts and showed superior tumor contrast compared to [^{89}Zr]Zr-DFO-STM108. Specifically, 6 days post-injection, the tumor exhibited the highest uptake, with minimal bone uptake, highlighting the tracer's stability and its potential for PD-L1 imaging [221].

4. Future Directions

The future of PET imaging in breast cancer lies in the development of radiotracers that are more stable and highly specific, enhancing tumor contrast and targeting a broader range of biomarkers while minimizing off-target radiation. Efforts should focus on optimizing tracers distinguishing between established biomarkers, such as HER2 and ERα, and developing emerging targets, like ERβ and HER4, to better capture the molecular heterogeneity of breast cancer.

Addressing the challenges of radiotracer selection is critical. Antibody-based tracers are highly specific and valuable for evaluating antibody biodistribution and future radioimmunotherapy dosimetry, but they are hindered by long circulation times and limited tissue penetration. In contrast, small molecules, with their smaller size, faster clearance, better tissue penetration, and high binding affinity, provide a promising alternative despite issues like high kidney uptake. Isotope selection must also be addressed for labeling bioactive molecules: antibodies require long half-life isotopes such as ^{89}Zr and ^{52}Mn, while small molecules benefit from short half-life isotopes like ^{18}F and ^{68}Ga. Selected isotopes should possess low positron maximum energy and high frequency for optimal resolution, along with low-energy gamma emissions for radiation safety. Attention must also be given to prosthetic groups or chelators for better high labeling, conjugating efficiency, and stability, ensuring compatibility without compromising tracer bioactivity.

However, potential pitfalls such as off-target uptake must be addressed, as they contribute to false positives, increased radiation dose, and reduced tumor contrast. These include the following: tracer instability (e.g., free ^{18}F or ^{89}Zr in bone; free ^{52}Mn in the pancreas); metabolic pathways (e.g., liver metabolism for antibody or lipophilic tracers like hormone receptor tracers; kidney excretion for small molecules); physiological expression of targets in organs (e.g., HER2 in the liver [222] and ovary [223]; hormone receptors in the uterus, ovary and pituitary gland [224]; PD-L1 in lymphoid tissues; and VEGFR1 in the kidneys); and non-malignant conditions increasing target expression (e.g., VEGFR in atherosclerosis, post-stroke neovascularization, and PARP1 in fatty liver disease [225]). Moreover, limited tumor expression of certain targets, such as HER3, highlights the need for tracers with high affinity to achieve sufficient imaging.

Future research should prioritize innovations in tracer development, including the optimization of suitable isotope production, facile site-specific labeling methods, and pharmacokinetic improvements to enhance safety (addressing both immunogenicity and dosimetry concerns) and effectiveness. Establishing standardized protocols is essential to minimize false negatives and false positives while ensuring accurate biomarker stratification, prediction, and the timely monitoring of therapy responses. These advancements will drive the evolution of PET imaging, paving the way for more precise and effective personalized breast cancer therapies.

5. Conclusions

In conclusion, the ongoing evolution of PET imaging and the development of innovative radiotracers hold significant promise for enhancing the diagnosis, treatment, and monitoring of breast cancer. By focusing on improving tracer specificity, stability, and safety, future research can pave the way for more personalized and effective management strategies, ultimately improving patient outcomes.

Funding: This research received no external funding.

Conflicts of Interest: The author declares no conflicts of interest.

References

1. Lei, S.; Zheng, R.; Zhang, S.; Wang, S.; Chen, R.; Sun, K.; Zeng, H.; Zhou, J.; Wei, W. Global patterns of breast cancer incidence and mortality: A population-based cancer registry data analysis from 2000 to 2020. *Cancer Commun.* **2021**, *41*, 1183–1194. [CrossRef] [PubMed]
2. Giaquinto, A.N.; Sung, H.; Miller, K.D.; Kramer, J.L.; Newman, L.A.; Minihan, A.; Jemal, A.; Siegel, R.L. Breast Cancer Statistics, 2022. *CA Cancer J. Clin.* **2022**, *72*, 524–541. [CrossRef] [PubMed]
3. Goldhirsch, A.; Wood, W.C.; Coates, A.S.; Gelber, R.D.; Thürlimann, B.; Senn, H.J. Strategies for subtypes—Dealing with the diversity of breast cancer: Highlights of the St Gallen International Expert Consensus on the Primary Therapy of Early Breast Cancer 2011. *Ann. Oncol.* **2011**, *22*, 1736–1747. [CrossRef]
4. McCarthy, A.M.; Friebel-Klingner, T.; Ehsan, S.; He, W.; Welch, M.; Chen, J.; Kontos, D.; Domchek, S.M.; Conant, E.F.; Semine, A.; et al. Relationship of established risk factors with breast cancer subtypes. *Cancer Med.* **2021**, *10*, 6456–6467. [CrossRef] [PubMed]
5. McGuire, A.; Brown, J.A.; Malone, C.; McLaughlin, R.; Kerin, M.J. Effects of age on the detection and management of breast cancer. *Cancers* **2015**, *7*, 908–929. [CrossRef] [PubMed]
6. Ngô, T.M.; Lê, Á.N.; Đinh, D.P.H. The Impact of Chemotherapy on Cardiovascular Mortality across Breast Cancer Subtypes. *Curr. Oncol.* **2024**, *31*, 649–659. [CrossRef]
7. Nishikawa, Y.; Agatsuma, N.; Utsumi, T.; Funakoshi, T.; Mori, Y.; Nakamura, Y.; Hoshino, N.; Horimatsu, T.; Saito, T.; Kashihara, S.; et al. Medical care costs according to the stage and subtype of breast cancer in a municipal setting: A case study of Hachioji City, Japan. *Breast Cancer* **2024**, *31*, 105–115. [CrossRef]
8. Kennecke, H.; Yerushalmi, R.; Woods, R.; Cheang, M.C.; Voduc, D.; Speers, C.H.; Nielsen, T.O.; Gelmon, K. Metastatic behavior of breast cancer subtypes. *J. Clin. Oncol.* **2010**, *28*, 3271–3277. [CrossRef] [PubMed]
9. Guo, Y.; Arciero, C.A.; Jiang, R.; Behera, M.; Peng, L.; Li, X. Different Breast Cancer Subtypes Show Different Metastatic Patterns: A Study from A Large Public Database. *Asian Pac. J. Cancer Prev.* **2020**, *21*, 3587–3593. [CrossRef] [PubMed]
10. Gerlinger, M.; Swanton, C. How Darwinian models inform therapeutic failure initiated by clonal heterogeneity in cancer medicine. *Br. J. Cancer* **2010**, *103*, 1139–1143. [CrossRef] [PubMed]
11. Guo, L.; Kong, D.; Liu, J.; Zhan, L.; Luo, L.; Zheng, W.; Zheng, Q.; Chen, C.; Sun, S. Breast cancer heterogeneity and its implication in personalized precision therapy. *Exp. Hematol. Oncol.* **2023**, *12*, 3. [CrossRef] [PubMed]
12. Ndlovu, H.; Lawal, I.O.; Mokoala, K.M.G.; Sathekge, M.M. Imaging Molecular Targets and Metabolic Pathways in Breast Cancer for Improved Clinical Management: Current Practice and Future Perspectives. *Int. J. Mol. Sci.* **2024**, *25*, 1575. [CrossRef]
13. Zhu, J.-Y.; He, H.-L.; Jiang, X.-C.; Bao, H.-W.; Chen, F. Multimodal ultrasound features of breast cancers: Correlation with molecular subtypes. *BMC Med. Imaging* **2023**, *23*, 57. [CrossRef]
14. Jannusch, K.; Bittner, A.-K.; Bruckmann, N.M.; Morawitz, J.; Stieglitz, C.; Dietzel, F.; Quick, H.H.; Baba, H.A.; Herrmann, K.; Umutlu, L.; et al. Correlation between Imaging Markers Derived from PET/MRI and Invasive Acquired Biomarkers in Newly Diagnosed Breast Cancer. *Cancers* **2023**, *15*, 1651. [CrossRef]
15. Temerik, S.M.; Elwahab, S.M.A.; Wahman, M.M.; Ahmed, M.Y.; Elwanis, M.E.A. Relation between morphological features of initial breast MRI and breast cancer molecular subtypes. *Egypt. J. Radiol. Nucl. Med.* **2023**, *54*, 147. [CrossRef]
16. Shokeir, F.A.; Soliman, N.; Khater, A.; Bayoumi, D. Evaluation of molecular subtypes of breast cancer using MRI BI-RADS Lexicon. *Egypt. J. Radiol. Nucl. Med.* **2024**, *55*, 52. [CrossRef]
17. Chen, L.; Xiao, Z.; Fu, J.; Huang, J.; Lan, Y. The diagnostic performance of dual-layer spectral detector CT for distinguishing breast cancer biomarker expression and molecular subtypes. *Sci. Rep.* **2024**, *14*, 1500. [CrossRef] [PubMed]
18. de Mooij, C.M.; Ploumen, R.A.W.; Nelemans, P.J.; Mottaghy, F.M.; Smidt, M.L.; van Nijnatten, T.J.A. The influence of receptor expression and clinical subtypes on baseline [18F]FDG uptake in breast cancer: Systematic review and meta-analysis. *EJNMMI Res.* **2023**, *13*, 5. [CrossRef] [PubMed]
19. Wu, J.; Zhang, X.; Jia, Z.; Zhou, X.; Qi, R.; Ji, H.; Sun, J.; Sun, C.; Teng, Z.; Lu, G.; et al. Combined (18)F-FDG and (18)F-Alfatide II PET May Predict Luminal B (HER2 Negative) Subtype and Nonluminal Subtype of Invasive Breast Cancer. *Mol. Pharm.* **2022**, *19*, 3405–3411. [CrossRef]
20. Yoon, H.J.; Kang, K.W.; Chun, I.K.; Cho, N.; Im, S.A.; Jeong, S.; Lee, S.; Jung, K.C.; Lee, Y.S.; Jeong, J.M.; et al. Correlation of breast cancer subtypes, based on estrogen receptor, progesterone receptor, and HER2, with functional imaging parameters from ^{68}Ga-RGD PET/CT and ^{18}F-FDG PET/CT. *Eur. J. Nucl. Med. Mol. Imaging* **2014**, *41*, 1534–1543. [CrossRef]

21. Schwenck, J.; Sonanini, D.; Cotton, J.M.; Rammensee, H.G.; la Fougère, C.; Zender, L.; Pichler, B.J. Advances in PET imaging of cancer. *Nat. Rev. Cancer* **2023**, *23*, 474–490. [CrossRef]
22. Gutierrez, C.; Schiff, R. HER2: Biology, detection, and clinical implications. *Arch. Pathol. Lab. Med.* **2011**, *135*, 55–62. [CrossRef] [PubMed]
23. Kang, B.; Lee, J.; Jung, J.H.; Kim, W.W.; Keum, H.; Park, H.Y. Differences in clinical outcomes between HER2-negative and HER2-positive luminal B breast cancer. *Medicine* **2023**, *102*, e34772. [CrossRef]
24. Press, D.J.; Miller, M.E.; Liederbach, E.; Yao, K.; Huo, D. De novo metastasis in breast cancer: Occurrence and overall survival stratified by molecular subtype. *Clin. Exp. Metastasis* **2017**, *34*, 457–465. [CrossRef] [PubMed]
25. Lin, M.; Luo, T.; Jin, Y.; Zhong, X.; Zheng, D.; Zeng, C.; Guo, Q.; Wu, J.; Shao, Z.-M.; Hu, X.; et al. HER2-low heterogeneity between primary and paired recurrent/metastatic breast cancer: Implications in treatment and prognosis. *Cancer* **2024**, *130*, 851–862. [CrossRef] [PubMed]
26. Hou, Y.; Nitta, H.; Li, Z. HER2 Intratumoral Heterogeneity in Breast Cancer, an Evolving Concept. *Cancers* **2023**, *15*, 2664. [CrossRef]
27. Tanei, T.; Seno, S.; Sota, Y.; Hatano, T.; Kitahara, Y.; Abe, K.; Masunaga, N.; Tsukabe, M.; Yoshinami, T.; Miyake, T.; et al. High HER2 Intratumoral Heterogeneity Is a Predictive Factor for Poor Prognosis in Early-Stage and Locally Advanced HER2-Positive Breast Cancer. *Cancers* **2024**, *16*, 1062. [CrossRef] [PubMed]
28. Shirman, Y.; Lubovsky, S.; Shai, A. HER2-Low Breast Cancer: Current Landscape and Future Prospects. *Breast Cancer: Targets Ther.* **2023**, *15*, 605–616. [CrossRef] [PubMed]
29. Bensch, F.; Brouwers, A.H.; Lub-de Hooge, M.N.; de Jong, J.R.; van der Vegt, B.; Sleijfer, S.; de Vries, E.G.E.; Schröder, C.P. 89Zr-trastuzumab PET supports clinical decision making in breast cancer patients, when HER2 status cannot be determined by standard work up. *Eur. J. Nucl. Med. Mol. Imaging* **2018**, *45*, 2300–2306. [CrossRef] [PubMed]
30. Ulaner, G.A.; Hyman, D.M.; Ross, D.S.; Corben, A.; Chandarlapaty, S.; Goldfarb, S.; McArthur, H.; Erinjeri, J.P.; Solomon, S.B.; Kolb, H.; et al. Detection of HER2-Positive Metastases in Patients with HER2-Negative Primary Breast Cancer Using 89Zr-Trastuzumab PET/CT. *J. Nucl. Med.* **2016**, *57*, 1523–1528. [CrossRef] [PubMed]
31. Dehdashti, F.; Wu, N.; Bose, R.; Naughton, M.J.; Ma, C.X.; Marquez-Nostra, B.V.; Diebolder, P.; Mpoy, C.; Rogers, B.E.; Lapi, S.E.; et al. Evaluation of [89Zr]trastuzumab-PET/CT in differentiating HER2-positive from HER2-negative breast cancer. *Breast Cancer Res. Treat.* **2018**, *169*, 523–530. [CrossRef]
32. Dijkers, E.C.; Oude Munnink, T.H.; Kosterink, J.G.; Brouwers, A.H.; Jager, P.L.; de Jong, J.R.; van Dongen, G.A.; Schröder, C.P.; Lub-de Hooge, M.N.; de Vries, E.G. Biodistribution of 89Zr-trastuzumab and PET Imaging of HER2-Positive Lesions in Patients With Metastatic Breast Cancer. *Clin. Pharmacol. Ther.* **2010**, *87*, 586–592. [CrossRef] [PubMed]
33. Ulaner, G.A.; Hyman, D.M.; Lyashchenko, S.K.; Lewis, J.S.; Carrasquillo, J.A. 89Zr-Trastuzumab PET/CT for Detection of Human Epidermal Growth Factor Receptor 2-Positive Metastases in Patients With Human Epidermal Growth Factor Receptor 2-Negative Primary Breast Cancer. *Clin. Nucl. Med.* **2017**, *42*, 912–917. [CrossRef] [PubMed]
34. Linders, D.G.J.; Deken, M.M.; van Dam, M.A.; Wasser, M.; Voormolen, E.M.C.; Kroep, J.R.; van Dongen, G.; Vugts, D.; Oosterkamp, H.M.; Straver, M.E.; et al. (89)Zr-Trastuzumab PET/CT Imaging of HER2-Positive Breast Cancer for Predicting Pathological Complete Response after Neoadjuvant Systemic Therapy: A Feasibility Study. *Cancers* **2023**, *15*, 4980. [CrossRef] [PubMed]
35. Gebhart, G.; Lamberts, L.E.; Wimana, Z.; Garcia, C.; Emonts, P.; Ameye, L.; Stroobants, S.; Huizing, M.; Aftimos, P.; Tol, J.; et al. Molecular imaging as a tool to investigate heterogeneity of advanced HER2-positive breast cancer and to predict patient outcome under trastuzumab emtansine (T-DM1): The ZEPHIR trial. *Ann. Oncol.* **2016**, *27*, 619–624. [CrossRef] [PubMed]
36. Mileva, M.; de Vries, E.G.E.; Guiot, T.; Wimana, Z.; Deleu, A.-L.; Schröder, C.P.; Lefebvre, Y.; Paesmans, M.; Stroobants, S.; Huizing, M.; et al. Molecular imaging predicts lack of T-DM1 response in advanced HER2-positive breast cancer (final results of ZEPHIR trial). *npj Breast Cancer* **2024**, *10*, 4. [CrossRef]
37. Gaykema, S.B.; Schröder, C.P.; Vitfell-Rasmussen, J.; Chua, S.; Oude Munnink, T.H.; Brouwers, A.H.; Bongaerts, A.H.; Akimov, M.; Fernandez-Ibarra, C.; Lub-de Hooge, M.N.; et al. 89Zr-trastuzumab and 89Zr-bevacizumab PET to evaluate the effect of the HSP90 inhibitor NVP-AUY922 in metastatic breast cancer patients. *Clin. Cancer Res.* **2014**, *20*, 3945–3954. [CrossRef] [PubMed]
38. McKnight, B.N.; Viola-Villegas, N.T. Monitoring Src status after dasatinib treatment in HER2+ breast cancer with (89)Zr-trastuzumab PET imaging. *Breast Cancer Res.* **2018**, *20*, 130. [CrossRef]
39. Deri, M.A.; Ponnala, S.; Kozlowski, P.; Burton-Pye, B.P.; Cicek, H.T.; Hu, C.; Lewis, J.S.; Francesconi, L.C. p-SCN-Bn-HOPO: A Superior Bifunctional Chelator for (89)Zr ImmunoPET. *Bioconjugate Chem.* **2015**, *26*, 2579–2591. [CrossRef] [PubMed]
40. Chomet, M.; Schreurs, M.; Bolijn, M.J.; Verlaan, M.; Beaino, W.; Brown, K.; Poot, A.J.; Windhorst, A.D.; Gill, H.; Marik, J.; et al. Head-to-head comparison of DFO* and DFO chelators: Selection of the best candidate for clinical (89)Zr-immuno-PET. *Eur. J. Nucl. Med. Mol. Imaging* **2021**, *48*, 694–707. [CrossRef]
41. Vivier, D.; Sharma, S.K.; Adumeau, P.; Rodriguez, C.; Fung, K.; Zeglis, B.M. The Impact of FcγRI Binding on Immuno-PET. *J. Nucl. Med.* **2019**, *60*, 1174–1182. [CrossRef] [PubMed]
42. Badier, L.; Quelven, I. Zirconium 89 and Copper 64 for ImmunoPET: From Antibody Bioconjugation and Radiolabeling to Molecular Imaging. *Pharmaceutics* **2024**, *16*, 882. [CrossRef]
43. Mortimer, J.E.; Bading, J.R.; Colcher, D.M.; Conti, P.S.; Frankel, P.H.; Carroll, M.I.; Tong, S.; Poku, E.; Miles, J.K.; Shively, J.E.; et al. Functional imaging of human epidermal growth factor receptor 2-positive metastatic breast cancer using (64)Cu-DOTA-trastuzumab PET. *J. Nucl. Med.* **2014**, *55*, 23–29. [CrossRef] [PubMed]

44. Carrasquillo, J.A.; Morris, P.G.; Humm, J.L.; Smith-Jones, P.M.; Beylergil, V.; Akhurst, T.; O'Donoghue, J.A.; Ruan, S.; Modi, S.; Hudis, C.A.; et al. Copper-64 trastuzumab PET imaging: A reproducibility study. *Q. J. Nucl. Med. Mol. Imaging* **2019**, *63*, 191–198. [CrossRef] [PubMed]
45. Kurihara, H.; Hamada, A.; Yoshida, M.; Shimma, S.; Hashimoto, J.; Yonemori, K.; Tani, H.; Miyakita, Y.; Kanayama, Y.; Wada, Y.; et al. (64)Cu-DOTA-trastuzumab PET imaging and HER2 specificity of brain metastases in HER2-positive breast cancer patients. *EJNMMI Res.* **2015**, *5*, 8. [CrossRef] [PubMed]
46. Mortimer, J.E.; Bading, J.R.; Frankel, P.H.; Carroll, M.I.; Yuan, Y.; Park, J.M.; Tumyan, L.; Gidwaney, N.; Poku, E.K.; Shively, J.E.; et al. Use of (64)Cu-DOTA-Trastuzumab PET to Predict Response and Outcome of Patients Receiving Trastuzumab Emtansine for Metastatic Breast Cancer: A Pilot Study. *J. Nucl. Med.* **2022**, *63*, 1145–1148. [CrossRef]
47. Woo, S.K.; Jang, S.J.; Seo, M.J.; Park, J.H.; Kim, B.S.; Kim, E.J.; Lee, Y.J.; Lee, T.S.; An, G.I.; Song, I.H.; et al. Development of (64)Cu-NOTA-Trastuzumab for HER2 Targeting: A Radiopharmaceutical with Improved Pharmacokinetics for Human Studies. *J. Nucl. Med.* **2019**, *60*, 26–33. [CrossRef] [PubMed]
48. Lee, I.; Lim, I.; Byun, B.H.; Kim, B.I.; Choi, C.W.; Woo, S.K.; Kim, K.I.; Lee, K.C.; Kang, J.H.; Seong, M.K.; et al. A preliminary clinical trial to evaluate (64)Cu-NOTA-Trastuzumab as a positron emission tomography imaging agent in patients with breast cancer. *EJNMMI Res.* **2021**, *11*, 8. [CrossRef] [PubMed]
49. Maisonial-Besset, A.; Witkowski, T.; Quintana, M.; Besse, S.; Gaumet, V.; Cordonnier, A.; Alliot, C.; Vidal, A.; Denevault-Sabourin, C.; Tarrit, S.; et al. Synthesis and In Vitro Comparison of DOTA, NODAGA and 15-5 Macrocycles as Chelators for the (64)Cu-Labelling of Immunoconjugates. *Molecules* **2022**, *28*, 75. [CrossRef] [PubMed]
50. Brandt, M.; Cardinale, J.; Rausch, I.; Mindt, T.L. Manganese in PET imaging: Opportunities and challenges. *J. Label. Comp. Radiopharm.* **2019**, *62*, 541–551. [CrossRef]
51. Toàn, N.M.; Vágner, A.; Nagy, G.; Ország, G.; Nagy, T.; Csikos, C.; Váradi, B.; Sajtos, G.Z.; Kapus, I.; Szoboszlai, Z.; et al. [(52)Mn]Mn-BPPA-Trastuzumab: A Promising HER2-Specific PET Radiotracer. *J. Med. Chem.* **2024**, *67*, 8261–8270. [CrossRef] [PubMed]
52. Omweri, J.M.; Saini, S.; Houson, H.A.; Tekin, V.; Pyles, J.M.; Parker, C.C.; Lapi, S.E. Development of (52)Mn Labeled Trastuzumab for Extended Time Point PET Imaging of HER2. *Mol. Imaging Biol.* **2024**, *26*, 858–868. [CrossRef]
53. Marquez, B.V.; Ikotun, O.F.; Zheleznyak, A.; Wright, B.; Hari-Raj, A.; Pierce, R.A.; Lapi, S.E. Evaluation of (89)Zr-pertuzumab in Breast cancer xenografts. *Mol. Pharm.* **2014**, *11*, 3988–3995. [CrossRef] [PubMed]
54. Ulaner, G.A.; Lyashchenko, S.K.; Riedl, C.; Ruan, S.; Zanzonico, P.B.; Lake, D.; Jhaveri, K.; Zeglis, B.; Lewis, J.S.; O'Donoghue, J.A. First-in-Human Human Epidermal Growth Factor Receptor 2-Targeted Imaging Using (89)Zr-Pertuzumab PET/CT: Dosimetry and Clinical Application in Patients with Breast Cancer. *J. Nucl. Med.* **2018**, *59*, 900–906. [CrossRef] [PubMed]
55. Massicano, A.V.F.; Lee, S.; Crenshaw, B.K.; Aweda, T.A.; El Sayed, R.; Super, I.; Bose, R.; Marquez-Nostra, B.V.; Lapi, S.E. Imaging of HER2 with [(89)Zr]pertuzumab in Response to T-DM1 Therapy. *Cancer Biother. Radiopharm.* **2019**, *34*, 209–217. [CrossRef] [PubMed]
56. Kang, M.; Shin, J.I.; Han, S.; Kim, J.Y.; Park, J.; Kim, K.I.; Kang, J.H.; Lee, T.S. Therapeutic Response Monitoring with (89)Zr-DFO-Pertuzumab in HER2-Positive and Trastuzumab-Resistant Breast Cancer Models. *Pharmaceutics* **2022**, *14*, 1338. [CrossRef] [PubMed]
57. Lu, Y.; Li, M.; Massicano, A.V.F.; Song, P.N.; Mansur, A.; Heinzman, K.A.; Larimer, B.M.; Lapi, S.E.; Sorace, A.G. [(89)Zr]-Pertuzumab PET Imaging Reveals Paclitaxel Treatment Efficacy Is Positively Correlated with HER2 Expression in Human Breast Cancer Xenograft Mouse Models. *Molecules* **2021**, *26*, 1568. [CrossRef] [PubMed]
58. Vivier, D.; Fung, K.; Rodriguez, C.; Adumeau, P.; Ulaner, G.A.; Lewis, J.S.; Sharma, S.K.; Zeglis, B.M. The Influence of Glycans-Specific Bioconjugation on the FcγRI Binding and In vivo Performance of (89)Zr-DFO-Pertuzumab. *Theranostics* **2020**, *10*, 1746–1757. [CrossRef] [PubMed]
59. Yeh, R.; O'Donoghue, J.A.; Jayaprakasam, V.S.; Mauguen, A.; Min, R.; Park, S.; Brockway, J.P.; Bromberg, J.F.; Zhi, W.I.; Robson, M.E.; et al. First-in-Human Evaluation of Site-Specifically Labeled (89)Zr-Pertuzumab in Patients with HER2-Positive Breast Cancer. *J. Nucl. Med.* **2024**, *65*, 386–393. [CrossRef]
60. Al-Saden, N.; Lam, K.; Chan, C.; Reilly, R.M. Positron-Emission Tomography of HER2-Positive Breast Cancer Xenografts in Mice with (89)Zr-Labeled Trastuzumab-DM1: A Comparison with (89)Zr-Labeled Trastuzumab. *Mol. Pharm.* **2018**, *15*, 3383–3393. [CrossRef] [PubMed]
61. Al-Saden, N.; Cai, Z.; Reilly, R.M. Tumor uptake and tumor/blood ratios for [(89)Zr]Zr-DFO-trastuzumab-DM1 on microPET/CT images in NOD/SCID mice with human breast cancer xenografts are directly correlated with HER2 expression and response to trastuzumab-DM1. *Nucl. Med. Biol.* **2018**, *67*, 43–51. [CrossRef] [PubMed]
62. Suman, S.K.; Mukherjee, A.; Pandey, U.; Chakraborty, A.; Rakshit, S.; Tawate, M.; Sarma, H.D. (68)Ga-Labeled Trastuzumab Fragments for ImmunoPET Imaging of Human Epidermal Growth Factor Receptor 2 Expression in Solid Cancers. *Cancer Biother. Radiopharm.* **2023**, *38*, 38–50. [CrossRef] [PubMed]
63. Moreau, M.; Poty, S.; Vrigneaud, J.M.; Walker, P.; Guillemin, M.; Raguin, O.; Oudot, A.; Bernhard, C.; Goze, C.; Boschetti, F.; et al. MANOTA: A promising bifunctional chelating agent for copper-64 immunoPET. *Dalton Trans.* **2017**, *46*, 14659–14668. [CrossRef]
64. Yue, T.T.C.; Ge, Y.; Aprile, F.A.; Ma, M.T.; Pham, T.T.; Long, N.J. Site-Specific (68)Ga Radiolabeling of Trastuzumab Fab via Methionine for ImmunoPET Imaging. *Bioconjugate Chem.* **2023**, *34*, 1802–1810. [CrossRef] [PubMed]

65. Mendler, C.T.; Gehring, T.; Wester, H.J.; Schwaiger, M.; Skerra, A. ^{89}Zr-Labeled Versus ^{124}I-Labeled αHER2 Fab with Optimized Plasma Half-Life for High-Contrast Tumor Imaging In Vivo. *J. Nucl. Med.* **2015**, *56*, 1112–1118. [CrossRef] [PubMed]
66. Richter, A.; Knorr, K.; Schlapschy, M.; Robu, S.; Morath, V.; Mendler, C.; Yen, H.Y.; Steiger, K.; Kiechle, M.; Weber, W.; et al. First In-Human Medical Imaging with a PASylated (89)Zr-Labeled Anti-HER2 Fab-Fragment in a Patient with Metastatic Breast Cancer. *Nucl. Med. Mol. Imaging* **2020**, *54*, 114–119. [CrossRef] [PubMed]
67. Zhou, Z.; McDougald, D.; Devoogdt, N.; Zalutsky, M.R.; Vaidyanathan, G. Labeling Single Domain Antibody Fragments with Fluorine-18 Using 2,3,5,6-Tetrafluorophenyl 6-[(18)F]Fluoronicotinate Resulting in High Tumor-to-Kidney Ratios. *Mol. Pharm.* **2019**, *16*, 214–226. [CrossRef] [PubMed]
68. Keyaerts, M.; Xavier, C.; Heemskerk, J.; Devoogdt, N.; Everaert, H.; Ackaert, C.; Vanhoeij, M.; Duhoux, F.P.; Gevaert, T.; Simon, P.; et al. Phase I Study of 68Ga-HER2-Nanobody for PET/CT Assessment of HER2 Expression in Breast Carcinoma. *J. Nucl. Med.* **2016**, *57*, 27–33. [CrossRef]
69. Gondry, O.; Caveliers, V.; Xavier, C.; Raes, L.; Vanhoeij, M.; Verfaillie, G.; Fontaine, C.; Glorieus, K.; De Grève, J.; Joris, S.; et al. Phase II Trial Assessing the Repeatability and Tumor Uptake of [(68)Ga]Ga-HER2 Single-Domain Antibody PET/CT in Patients with Breast Carcinoma. *J. Nucl. Med.* **2024**, *65*, 178–184. [CrossRef] [PubMed]
70. Ducharme, M.; Hall, L.; Eckenroad, W.; Cingoranelli, S.J.; Houson, H.A.; Jaskowski, L.; Hunter, C.; Larimer, B.M.; Lapi, S.E. Evaluation of [(89)Zr]Zr-DFO-2Rs15d Nanobody for Imaging of HER2-Positive Breast Cancer. *Mol. Pharm.* **2023**, *20*, 4629–4639. [CrossRef]
71. Luo, R.; Liu, H.; Cheng, Z. Protein scaffolds: Antibody alternatives for cancer diagnosis and therapy. *RSC Chem. Biol.* **2022**, *3*, 830–847. [CrossRef] [PubMed]
72. Ahlgren, S.; Orlova, A.; Rosik, D.; Sandström, M.; Sjöberg, A.; Baastrup, B.; Widmark, O.; Fant, G.; Feldwisch, J.; Tolmachev, V. Evaluation of maleimide derivative of DOTA for site-specific labeling of recombinant affibody molecules. *Bioconjugate Chem.* **2008**, *19*, 235–243. [CrossRef] [PubMed]
73. Feldwisch, J.; Tolmachev, V.; Lendel, C.; Herne, N.; Sjöberg, A.; Larsson, B.; Rosik, D.; Lindqvist, E.; Fant, G.; Höidén-Guthenberg, I.; et al. Design of an optimized scaffold for affibody molecules. *J. Mol. Biol.* **2010**, *398*, 232–247. [CrossRef] [PubMed]
74. Sandström, M.; Lindskog, K.; Velikyan, I.; Wennborg, A.; Feldwisch, J.; Sandberg, D.; Tolmachev, V.; Orlova, A.; Sörensen, J.; Carlsson, J.; et al. Biodistribution and Radiation Dosimetry of the Anti-HER2 Affibody Molecule 68Ga-ABY-025 in Breast Cancer Patients. *J. Nucl. Med.* **2016**, *57*, 867–871. [CrossRef]
75. Sandberg, D.; Tolmachev, V.; Velikyan, I.; Olofsson, H.; Wennborg, A.; Feldwisch, J.; Carlsson, J.; Lindman, H.; Sörensen, J. Intra-image referencing for simplified assessment of HER2-expression in breast cancer metastases using the Affibody molecule ABY-025 with PET and SPECT. *Eur. J. Nucl. Med. Mol. Imaging* **2017**, *44*, 1337–1346. [CrossRef] [PubMed]
76. Sörensen, J.; Velikyan, I.; Sandberg, D.; Wennborg, A.; Feldwisch, J.; Tolmachev, V.; Orlova, A.; Sandström, M.; Lubberink, M.; Olofsson, H.; et al. Measuring HER2-Receptor Expression In Metastatic Breast Cancer Using [68Ga]ABY-025 Affibody PET/CT. *Theranostics* **2016**, *6*, 262–271. [CrossRef] [PubMed]
77. Altena, R.; Burén, S.A.; Blomgren, A.; Karlsson, E.; Tzortzakakis, A.; Brun, N.; Moein, M.M.; Jussing, E.; Frejd, F.Y.; Bergh, J.; et al. Human Epidermal Growth Factor Receptor 2 (HER2) PET Imaging of HER2-Low Breast Cancer with [(68)Ga]Ga-ABY-025: Results from a Pilot Study. *J. Nucl. Med.* **2024**, *65*, 700–707. [CrossRef] [PubMed]
78. Alhuseinalkhudhur, A.; Lindman, H.; Liss, P.; Sundin, T.; Frejd, F.Y.; Hartman, J.; Iyer, V.; Feldwisch, J.; Lubberink, M.; Rönnlund, C.; et al. Human Epidermal Growth Factor Receptor 2-Targeting [(68)Ga]Ga-ABY-025 PET/CT Predicts Early Metabolic Response in Metastatic Breast Cancer. *J. Nucl. Med.* **2023**, *64*, 1364–1370. [CrossRef]
79. Xu, Y.; Bai, Z.; Huang, Q.; Pan, Y.; Pan, D.; Wang, L.; Yan, J.; Wang, X.; Yang, R.; Yang, M. PET of HER2 Expression with a Novel (18)FAl Labeled Affibody. *J. Cancer* **2017**, *8*, 1170–1178. [CrossRef]
80. Xu, Y.; Wang, L.; Pan, D.; Yu, C.; Mi, B.; Huang, Q.; Sheng, J.; Yan, J.; Wang, X.; Yang, R.; et al. PET imaging of a (68)Ga labeled modified HER2 affibody in breast cancers: From xenografts to patients. *Br. J. Radiol.* **2019**, *92*, 20190425. [CrossRef]
81. Xu, Y.; Wang, L.; Pan, D.; Yan, J.; Wang, X.; Yang, R.; Li, M.; Liu, Y.; Yang, M. Synthesis of a novel (89)Zr-labeled HER2 affibody and its application study in tumor PET imaging. *EJNMMI Res.* **2020**, *10*, 58. [CrossRef] [PubMed]
82. Liu, Y.; Xu, T.; Vorobyeva, A.; Loftenius, A.; Bodenko, V.; Orlova, A.; Frejd, F.Y.; Tolmachev, V. Radionuclide Therapy of HER2-Expressing Xenografts Using [(177)Lu]Lu-ABY-027 Affibody Molecule Alone and in Combination with Trastuzumab. *Cancers* **2023**, *15*, 2409. [CrossRef]
83. Oroujeni, M.; Rinne, S.S.; Vorobyeva, A.; Loftenius, A.; Feldwisch, J.; Jonasson, P.; Chernov, V.; Orlova, A.; Frejd, F.Y.; Tolmachev, V. Preclinical Evaluation of 99mTc-ZHER2:41071, a Second-Generation Affibody-Based HER2-Visualizing Imaging Probe with a Low Renal Uptake. *Int. J. Mol. Sci.* **2021**, *22*, 2770. [CrossRef]
84. von Witting, E.; Garousi, J.; Lindbo, S.; Vorobyeva, A.; Altai, M.; Oroujeni, M.; Mitran, B.; Orlova, A.; Hober, S.; Tolmachev, V. Selection of the optimal macrocyclic chelators for labeling with (111)In and (68)Ga improves contrast of HER2 imaging using engineered scaffold protein ADAPT6. *Eur. J. Pharm. Biopharm.* **2019**, *140*, 109–120. [CrossRef] [PubMed]
85. Fay, R.; Törő, I.; Schinke, A.L.; Simic, B.; Schaefer, J.V.; Dreier, B.; Plückthun, A.; Holland, J.P. Sortase-Mediated Site-Specific Conjugation and (89)Zr-Radiolabeling of Designed Ankyrin Repeat Proteins for PET. *Mol. Pharm.* **2022**, *19*, 3576–3585. [CrossRef] [PubMed]

86. Altunay, B.; Morgenroth, A.; Beheshti, M.; Vogg, A.; Wong, N.C.L.; Ting, H.H.; Biersack, H.J.; Stickeler, E.; Mottaghy, F.M. HER2-directed antibodies, affibodies and nanobodies as drug-delivery vehicles in breast cancer with a specific focus on radioimmunotherapy and radioimmunoimaging. *Eur. J. Nucl. Med. Mol. Imaging* **2021**, *48*, 1371–1389. [CrossRef]
87. Cavallaro, P.A.; De Santo, M.; Belsito, E.L.; Longobucco, C.; Curcio, M.; Morelli, C.; Pasqua, L.; Leggio, A. Peptides Targeting HER2-Positive Breast Cancer Cells and Applications in Tumor Imaging and Delivery of Chemotherapeutics. *Nanomaterials* **2023**, *13*, 2476. [CrossRef] [PubMed]
88. Ducharme, M.; Lapi, S.E. Peptide Based Imaging Agents for HER2 Imaging in Oncology. *Mol. Imaging* **2020**, *19*, 1536012120960258. [CrossRef] [PubMed]
89. Biabani Ardakani, J.; Akhlaghi, M.; Nikkholgh, B.; Hosseinimehr, S.J. Targeting and imaging of HER2 overexpression tumor with a new peptide-based (68)Ga-PET radiotracer. *Bioorganic Chem.* **2021**, *106*, 104474. [CrossRef] [PubMed]
90. Ducharme, M.; Houson, H.A.; Fernandez, S.R.; Lapi, S.E. Evaluation of 68Ga-Radiolabeled Peptides for HER2 PET Imaging. *Diagnostics* **2022**, *12*, 2710. [CrossRef] [PubMed]
91. de Roode, K.E.; Joosten, L.; Behe, M. Towards the Magic Radioactive Bullet: Improving Targeted Radionuclide Therapy by Reducing the Renal Retention of Radioligands. *Pharmaceuticals* **2024**, *17*, 256. [CrossRef]
92. Jiang, Z.; Guo, J.; Shen, J.; Jin, M.; Xie, S.; Wang, L. The role of estrogen receptor alpha in mediating chemoresistance in breast cancer cells. *J. Exp. Clin. Cancer Res.* **2012**, *31*, 42. [CrossRef] [PubMed]
93. Miziak, P.; Baran, M.; Błaszczak, E.; Przybyszewska-Podstawka, A.; Kałafut, J.; Smok-Kalwat, J.; Dmoszyńska-Graniczka, M.; Kiełbus, M.; Stepulak, A. Estrogen Receptor Signaling in Breast Cancer. *Cancers* **2023**, *15*, 4689. [CrossRef]
94. Sperduto, P.W.; Mesko, S.; Li, J.; Cagney, D.; Aizer, A.; Lin, N.U.; Nesbit, E.; Kruser, T.J.; Chan, J.; Braunstein, S.; et al. Estrogen/progesterone receptor and HER2 discordance between primary tumor and brain metastases in breast cancer and its effect on treatment and survival. *Neuro Oncol.* **2020**, *22*, 1359–1367. [CrossRef] [PubMed]
95. Yoshida, T.; Eguchi, H.; Nakachi, K.; Tanimoto, K.; Higashi, Y.; Suemasu, K.; Iino, Y.; Morishita, Y.; Hayashi, S.-i. Distinct mechanisms of loss of estrogen receptor α gene expression in human breast cancer: Methylation of the gene and alteration of trans-acting factors. *Carcinogenesis* **2000**, *21*, 2193–2201. [CrossRef] [PubMed]
96. Hartkopf, A.D.; Grischke, E.M.; Brucker, S.Y. Endocrine-Resistant Breast Cancer: Mechanisms and Treatment. *Breast Care* **2020**, *15*, 347–354. [CrossRef]
97. Liu, C.; Ma, G.; Xu, X.; Song, S.; Yang, Z. Can 18F-FES PET Improve the Evaluation of 18F-FDG PET in Patients With Metastatic Invasive Lobular Carcinoma? *Clin. Nucl. Med.* **2024**, *49*, 301–307. [CrossRef] [PubMed]
98. Kiatkittikul, P.; Mayurasakorn, S.; Promteangtrong, C.; Kunawudhi, A.; Siripongsatian, D.; Hirata, N.; Jantarato, A.; Boonkawin, N.; Yaset, S.; Kongsakorn, P.; et al. Head-to-head comparison of (18)F-FDG and (18)F-FES PET/CT for initial staging of ER-positive breast cancer patients. *Eur. J. Hybrid Imaging* **2023**, *7*, 23. [CrossRef] [PubMed]
99. Piccardo, A.; Fiz, F.; Treglia, G.; Bottoni, G.; Trimboli, P. Head-to-Head Comparison between (18)F-FES PET/CT and (18)F-FDG PET/CT in Oestrogen Receptor-Positive Breast Cancer: A Systematic Review and Meta-Analysis. *J. Clin. Med.* **2022**, *11*, 1919. [CrossRef] [PubMed]
100. Iqbal, R.; Yaqub, M.; Bektas, H.O.; Oprea-Lager, D.E.; de Vries, E.G.E.; Glaudemans, A.; Aftimos, P.; Gebhart, G.; Beelen, A.P.; Schuit, R.C.; et al. [18F]FDG and [18F]FES PET/CT Imaging as a Biomarker for Therapy Effect in Patients with Metastatic ER+ Breast Cancer Undergoing Treatment with Rintodestrant. *Clin. Cancer Res.* **2023**, *29*, 2075–2084. [CrossRef] [PubMed]
101. He, M.; Liu, C.; Shi, Q.; Sun, Y.; Zhang, Y.; Xu, X.; Yuan, H.; Zhang, Y.; Liu, Y.; Liu, G.; et al. The Predictive Value of Early Changes in (18) F-Fluoroestradiol Positron Emission Tomography/Computed Tomography During Fulvestrant 500 mg Therapy in Patients with Estrogen Receptor-Positive Metastatic Breast Cancer. *Oncologist* **2020**, *25*, 927–936. [CrossRef] [PubMed]
102. You, S.; Xie, Y.; Ji, M.; Liu, C.; Zhao, Y.; Gong, C.; Hu, S.; Li, Y.; Yang, Z.; Wang, B. ER status conversion and subsequent treatment: An assessment of negative ER expression detected by 18F-FES PET in metastatic breast cancer patients with ER-positive primary tumors. *Ther. Adv. Med. Oncol.* **2023**, *15*, 17588359231216093. [CrossRef] [PubMed]
103. Liu, S.; Gu, B.; Zhang, J.; Zhang, Y.; Xu, X.; Yuan, H.; Zhang, Y.; Yang, Z. The feasibility of (18)F-FES and (18)F-FDG microPET/CT for early monitoring the effect of fulvestrant on sensitizing docetaxel by downregulating ERα in ERα+ breast cancer. *Ann. Nucl. Med.* **2018**, *32*, 272–280. [CrossRef] [PubMed]
104. Gennari, A.; Brain, E.; De Censi, A.; Nanni, O.; Wuerstlein, R.; Frassoldati, A.; Cortes, J.; Rossi, V.; Palleschi, M.; Alberini, J.L.; et al. Early prediction of endocrine responsiveness in ER+/HER2-negative metastatic breast cancer (MBC): Pilot study with (18)F-fluoroestradiol ((18)F-FES) CT/PET. *Ann. Oncol.* **2024**, *35*, 549–558. [CrossRef] [PubMed]
105. Peterson, L.M.; Kurland, B.F.; Yan, F.; Jiresova, A.N.; Gadi, V.K.; Specht, J.M.; Gralow, J.R.; Schubert, E.K.; Link, J.M.; Krohn, K.A.; et al. (18)F-Fluoroestradiol PET Imaging in a Phase II Trial of Vorinostat to Restore Endocrine Sensitivity in ER+/HER2- Metastatic Breast Cancer. *J. Nucl. Med.* **2021**, *62*, 184–190. [CrossRef]
106. Liu, C.; Hu, S.; Xu, X.; Zhang, Y.; Wang, B.; Song, S.; Yang, Z. Evaluation of tumour heterogeneity by (18)F-fluoroestradiol PET as a predictive measure in breast cancer patients receiving palbociclib combined with endocrine treatment. *Breast Cancer Res.* **2022**, *24*, 57. [CrossRef]
107. Paquette, M.; Phoenix, S.; Ouellet, R.; Langlois, R.; van Lier, J.E.; Turcotte, E.E.; Bénard, F.; Lecomte, R. Assessment of the novel estrogen receptor PET tracer 4-fluoro-11β-methoxy-16α-[(18)F]fluoroestradiol (4FMFES) by PET imaging in a breast cancer murine model. *Mol. Imaging Biol.* **2013**, *15*, 625–632. [CrossRef] [PubMed]

108. Paquette, M.; Espinosa-Bentancourt, E.; Lavallée, É.; Phoenix, S.; Lapointe-Milot, K.; Bessette, P.; Guérin, B.; Turcotte, É.E. (18)F-4FMFES and (18)F-FDG PET/CT in Estrogen Receptor-Positive Endometrial Carcinomas: Preliminary Report. *J. Nucl. Med.* **2022**, *63*, 702–707. [CrossRef]
109. Paquette, M.; Lavallée, É.; Phoenix, S.; Ouellet, R.; Senta, H.; van Lier, J.E.; Guérin, B.; Lecomte, R.; Turcotte, É.E. Improved Estrogen Receptor Assessment by PET Using the Novel Radiotracer (18)F-4FMFES in Estrogen Receptor-Positive Breast Cancer Patients: An Ongoing Phase II Clinical Trial. *J. Nucl. Med.* **2018**, *59*, 197–203. [CrossRef]
110. Xu, D.; Lin, X.; Zeng, X.; Wen, X.; Li, J.; Li, Y.; Huang, J.; Chen, X.; Guo, Z.; Zhang, X. Radioiodinated 4-(p-Iodophenyl) Butanoic Acid-Modified Estradiol Derivative for ER Targeting SPECT Imaging. *Anal. Chem.* **2021**, *93*, 13998–14006. [CrossRef]
111. Liu, H.; Lin, X.; Xu, D.; Li, J.; Fang, J.; Li, J.; Meng, L.; Zeng, X.; Li, Y.; Huang, J.; et al. Radioiodinated Ethinylestradiol Derivatives for Estrogen Receptor Targeting Breast Cancer Imaging. *ACS Med. Chem. Lett.* **2022**, *13*, 203–210. [CrossRef] [PubMed]
112. Trabert, B.; Sherman, M.E.; Kannan, N.; Stanczyk, F.Z. Progesterone and Breast Cancer. *Endocr. Rev.* **2019**, *41*, 320–344. [CrossRef] [PubMed]
113. Pedroza, D.A.; Subramani, R.; Lakshmanaswamy, R. Classical and Non-Classical Progesterone Signaling in Breast Cancers. *Cancers* **2020**, *12*, 2440. [CrossRef]
114. Wei, S. Hormone receptors in breast cancer: An update on the uncommon subtypes. *Pathol.-Res. Pract.* **2023**, *250*, 154791. [CrossRef] [PubMed]
115. Fei, F.; Siegal, G.P.; Wei, S. Characterizing Clinicopathologic Features of Estrogen Receptor-Positive/Progesterone Receptor-Negative Breast Cancers. *Clin. Breast Cancer* **2022**, *22*, e788–e797. [CrossRef]
116. Lashen, A.G.; Toss, M.S.; Mongan, N.P.; Green, A.R.; Rakha, E.A. The clinical value of progesterone receptor expression in luminal breast cancer: A study of a large cohort with long-term follow-up. *Cancer* **2023**, *129*, 1183–1194. [CrossRef] [PubMed]
117. Salem, K.; Kumar, M.; Yan, Y.; Jeffery, J.J.; Kloepping, K.C.; Michel, C.J.; Powers, G.L.; Mahajan, A.M.; Fowler, A.M. Sensitivity and Isoform Specificity of ¹⁸F-Fluorofuranylnorprogesterone for Measuring Progesterone Receptor Protein Response to Estradiol Challenge in Breast Cancer. *J. Nucl. Med.* **2019**, *60*, 220–226. [CrossRef] [PubMed]
118. Dehdashti, F.; Laforest, R.; Gao, F.; Aft, R.L.; Dence, C.S.; Zhou, D.; Shoghi, K.I.; Siegel, B.A.; Katzenellenbogen, J.A.; Welch, M.J. Assessment of progesterone receptors in breast carcinoma by PET with 21-18F-fluoro-16α,17α-[(R)-(1′-α-furylmethylidene)dioxy]-19-norpregn-4-ene-3,20-dione. *J. Nucl. Med.* **2012**, *53*, 363–370. [CrossRef]
119. Chan, S.R.; Fowler, A.M.; Allen, J.A.; Zhou, D.; Dence, C.S.; Sharp, T.L.; Fettig, N.M.; Dehdashti, F.; Katzenellenbogen, J.A. Longitudinal noninvasive imaging of progesterone receptor as a predictive biomarker of tumor responsiveness to estrogen deprivation therapy. *Clin. Cancer Res.* **2015**, *21*, 1063–1070. [CrossRef] [PubMed]
120. Kumar, M.; Salem, K.; Jeffery, J.J.; Yan, Y.; Mahajan, A.M.; Fowler, A.M. Longitudinal Molecular Imaging of Progesterone Receptor Reveals Early Differential Response to Endocrine Therapy in Breast Cancer with an Activating ESR1 Mutation. *J. Nucl. Med.* **2021**, *62*, 500–506. [CrossRef] [PubMed]
121. Dehdashti, F.; Wu, N.; Ma, C.X.; Naughton, M.J.; Katzenellenbogen, J.A.; Siegel, B.A. Association of PET-based estradiol-challenge test for breast cancer progesterone receptors with response to endocrine therapy. *Nat. Commun.* **2021**, *12*, 733. [CrossRef] [PubMed]
122. Wu, X.; You, L.; Zhang, D.; Gao, M.; Li, Z.; Xu, D.; Zhang, P.; Huang, L.; Zhuang, R.; Wu, H.; et al. Synthesis and preliminary evaluation of a (18) F-labeled ethisterone derivative [(18) F]EAEF for progesterone receptor targeting. *Chem. Biol. Drug Des.* **2017**, *89*, 559–565. [CrossRef]
123. Lee, J.H.; Zhou, H.B.; Dence, C.S.; Carlson, K.E.; Welch, M.J.; Katzenellenbogen, J.A. Development of [F-18]fluorine-substituted Tanaproget as a progesterone receptor imaging agent for positron emission tomography. *Bioconjugate Chem.* **2010**, *21*, 1096–1104. [CrossRef]
124. Gao, F.; Peng, C.; Zhuang, R.; Guo, Z.; Liu, H.; Huang, L.; Li, H.; Xu, D.; Wen, X.; Fang, J.; et al. (18)F-labeled ethisterone derivative for progesterone receptor targeted PET imaging of breast cancer. *Nucl. Med. Biol.* **2019**, *72–73*, 62–69. [CrossRef] [PubMed]
125. Allott, L.; Miranda, C.; Hayes, A.; Raynaud, F.; Cawthorne, C.; Smith, G. Synthesis of a benzoxazinthione derivative of tanaproget and pharmacological evaluation for PET imaging of PR expression. *EJNMMI Radiopharm. Chem.* **2019**, *4*, 1. [CrossRef]
126. Davey, M.G.; Hynes, S.O.; Kerin, M.J.; Miller, N.; Lowery, A.J. Ki-67 as a Prognostic Biomarker in Invasive Breast Cancer. *Cancers* **2021**, *13*, 4455. [CrossRef]
127. Finkelman, B.S.; Zhang, H.; Hicks, D.G.; Turner, B.M. The Evolution of Ki-67 and Breast Carcinoma: Past Observations, Present Directions, and Future Considerations. *Cancers* **2023**, *15*, 808. [CrossRef] [PubMed]
128. Maranta, A.F.; Broder, S.; Fritzsche, C.; Knauer, M.; Thürlimann, B.; Jochum, W.; Ruhstaller, T. Do YOU know the Ki-67 index of your breast cancer patients? Knowledge of your institution's Ki-67 index distribution and its robustness is essential for decision-making in early breast cancer. *Breast* **2020**, *51*, 120–126. [CrossRef]
129. Soliman, N.A.; Yussif, S.M. Ki-67 as a prognostic marker according to breast cancer molecular subtype. *Cancer Biol. Med.* **2016**, *13*, 496–504. [CrossRef]
130. Zhao, J.; Wang, H. Correlation between (18) F-FDG PET/CT semiquantitative parameters and Ki-67 expression in pulmonary mucosa-associated lymphoid tissue lymphoma. *J. Med. Imaging Radiat. Oncol.* **2021**, *65*, 188–194. [CrossRef]
131. Mitamura, K.; Yamamoto, Y.; Norikane, T.; Hatakeyama, T.; Okada, M.; Nishiyama, Y. Correlation of (18)F-FDG and (11)C-methionine uptake on PET/CT with Ki-67 immunohistochemistry in newly diagnosed intracranial meningiomas. *Ann. Nucl. Med.* **2018**, *32*, 627–633. [CrossRef] [PubMed]

132. Deng, S.M.; Zhang, W.; Zhang, B.; Chen, Y.Y.; Li, J.H.; Wu, Y.W. Correlation between the Uptake of 18F-Fluorodeoxyglucose (18F-FDG) and the Expression of Proliferation-Associated Antigen Ki-67 in Cancer Patients: A Meta-Analysis. *PLoS ONE* **2015**, *10*, e0129028. [CrossRef] [PubMed]
133. Yamamoto, Y.; Ono, Y.; Aga, F.; Kawai, N.; Kudomi, N.; Nishiyama, Y. Correlation of 18F-FLT uptake with tumor grade and Ki-67 immunohistochemistry in patients with newly diagnosed and recurrent gliomas. *J. Nucl. Med.* **2012**, *53*, 1911–1915. [CrossRef] [PubMed]
134. Yu, W.; Su, X.; Zhang, D.; Qiao, F.; Wang, H.; Jiang, J.; Xu, H. Dual-Tracer Assessment of Dynamic Changes in Reoxygenation and Proliferation Decrease During Fractionated Radiotherapy in Murine Tumors. *Front. Oncol.* **2020**, *10*, 1046. [CrossRef]
135. Nakajo, M.; Nakajo, M.; Kajiya, Y.; Goto, Y.; Jinguji, M.; Tanaka, S.; Fukukura, Y.; Tani, A.; Higashi, M. Correlations of (18)F-fluorothymidine uptake with pathological tumour size, Ki-67 and thymidine kinase 1 expressions in primary and metastatic lymph node colorectal cancer foci. *Eur. Radiol.* **2014**, *24*, 3199–3209. [CrossRef] [PubMed]
136. Chalkidou, A.; Landau, D.B.; Odell, E.W.; Cornelius, V.R.; O'Doherty, M.J.; Marsden, P.K. Correlation between Ki-67 immunohistochemistry and 18F-fluorothymidine uptake in patients with cancer: A systematic review and meta-analysis. *Eur. J. Cancer* **2012**, *48*, 3499–3513. [CrossRef]
137. Surov, A.; Meyer, H.J.; Wienke, A. Associations Between PET Parameters and Expression of Ki-67 in Breast Cancer. *Transl. Oncol.* **2019**, *12*, 375–380. [CrossRef] [PubMed]
138. Sanghera, B.; Wong, W.L.; Sonoda, L.I.; Beynon, G.; Makris, A.; Woolf, D.; Ardeshna, K. FLT PET-CT in evaluation of treatment response. *Indian. J. Nucl. Med.* **2014**, *29*, 65–73. [CrossRef] [PubMed]
139. McDonald, E.S.; Doot, R.K.; Young, A.J.; Schubert, E.K.; Tchou, J.; Pryma, D.A.; Farwell, M.D.; Nayak, A.; Ziober, A.; Feldman, M.D.; et al. Breast Cancer (18)F-ISO-1 Uptake as a Marker of Proliferation Status. *J. Nucl. Med.* **2020**, *61*, 665–670. [CrossRef]
140. Masuda, H.; Zhang, D.; Bartholomeusz, C.; Doihara, H.; Hortobagyi, G.N.; Ueno, N.T. Role of epidermal growth factor receptor in breast cancer. *Breast Cancer Res. Treat.* **2012**, *136*, 331–345. [CrossRef] [PubMed]
141. Sirkisoon, S.R.; Carpenter, R.L.; Rimkus, T.; Miller, L.; Metheny-Barlow, L.; Lo, H.W. EGFR and HER2 signaling in breast cancer brain metastasis. *Front. Biosci.* **2016**, *8*, 245–263. [CrossRef]
142. Oshi, M.; Gandhi, S.; Tokumaru, Y.; Yan, L.; Yamada, A.; Matsuyama, R.; Ishikawa, T.; Endo, I.; Takabe, K. Conflicting roles of EGFR expression by subtypes in breast cancer. *Am. J. Cancer Res.* **2021**, *11*, 5094–5110. [PubMed]
143. Lee, H.J.; Seo, A.N.; Kim, E.J.; Jang, M.H.; Kim, Y.J.; Kim, J.H.; Kim, S.W.; Ryu, H.S.; Park, I.A.; Im, S.A.; et al. Prognostic and predictive values of EGFR overexpression and EGFR copy number alteration in HER2-positive breast cancer. *Br. J. Cancer* **2015**, *112*, 103–111. [CrossRef] [PubMed]
144. Sadri, K.; Ren, Q.; Zhang, K.; Paudyal, B.; Devadhas, D.; Rodeck, U.; Thakur, M. PET imaging of EGFR expression in nude mice bearing MDA-MB-468, a human breast adenocarcinoma. *Nucl. Med. Commun.* **2011**, *32*, 563–569. [CrossRef] [PubMed]
145. McKnight, B.N.; Kim, S.; Boerner, J.L.; Viola, N.T. Cetuximab PET delineated changes in cellular distribution of EGFR upon dasatinib treatment in triple negative breast cancer. *Breast Cancer Res.* **2020**, *22*, 37. [CrossRef] [PubMed]
146. Bhattacharyya, S.; Kurdziel, K.; Wei, L.; Riffle, L.; Kaur, G.; Hill, G.C.; Jacobs, P.M.; Tatum, J.L.; Doroshow, J.H.; Kalen, J.D. Zirconium-89 labeled panitumumab: A potential immuno-PET probe for HER1-expressing carcinomas. *Nucl. Med. Biol.* **2013**, *40*, 451–457. [CrossRef]
147. Cavaliere, A.; Sun, S.; Lee, S.; Bodner, J.; Li, Z.; Huang, Y.; Moores, S.L.; Marquez-Nostra, B. Development of [(89)Zr]ZrDFO-amivantamab bispecific to EGFR and c-MET for PET imaging of triple-negative breast cancer. *Eur. J. Nucl. Med. Mol. Imaging* **2021**, *48*, 383–394. [CrossRef]
148. Tikum, A.F.; Nambisan, A.K.; Ketchemen, J.P.; Babeker, H.; Khan, M.N.; Torlakovic, E.E.; Fonge, H. Simultaneous Imaging and Therapy Using Epitope-Specific Anti-Epidermal Growth Factor Receptor (EGFR) Antibody Conjugates. *Pharmaceutics* **2022**, *14*, 1917. [CrossRef] [PubMed]
149. Chekol, R.; Solomon, V.R.; Alizadeh, E.; Bernhard, W.; Fisher, D.; Hill, W.; Barreto, K.; DeCoteau, J.F.; Parada, A.C.; Geyer, C.R.; et al. (89)Zr-nimotuzumab for immunoPET imaging of epidermal growth factor receptor I. *Oncotarget* **2018**, *9*, 17117–17132. [CrossRef] [PubMed]
150. Solomon, V.R.; Barreto, K.; Bernhard, W.; Alizadeh, E.; Causey, P.; Perron, R.; Gendron, D.; Alam, M.K.; Carr, A.; Geyer, C.R.; et al. Nimotuzumab Site-Specifically Labeled with (89)Zr and (225)Ac Using SpyTag/SpyCatcher for PET Imaging and Alpha Particle Radioimmunotherapy of Epidermal Growth Factor Receptor Positive Cancers. *Cancers* **2020**, *12*, 3449. [CrossRef]
151. Alizadeh, E.; Behlol Ayaz Ahmed, K.; Raja Solomon, V.; Gaja, V.; Bernhard, W.; Makhlouf, A.; Gonzalez, C.; Barreto, K.; Casaco, A.; Geyer, C.R.; et al. (89)Zr-Labeled Domain II-Specific scFv-Fc ImmunoPET Probe for Imaging Epidermal Growth Factor Receptor In Vivo. *Cancers* **2021**, *13*, 560. [CrossRef]
152. Summer, D.; Garousi, J.; Oroujeni, M.; Mitran, B.; Andersson, K.G.; Vorobyeva, A.; Löfblom, J.; Orlova, A.; Tolmachev, V.; Decristoforo, C. Cyclic versus Noncyclic Chelating Scaffold for (89)Zr-Labeled ZEGFR:2377 Affibody Bioconjugates Targeting Epidermal Growth Factor Receptor Overexpression. *Mol. Pharm.* **2018**, *15*, 175–185. [CrossRef] [PubMed]
153. Dey, N.; Williams, C.; Leyland-Jones, B.; De, P. A critical role for HER3 in HER2-amplified and non-amplified breast cancers: Function of a kinase-dead RTK. *Am. J. Transl. Res.* **2015**, *7*, 733–750. [PubMed]
154. Uliano, J.; Corvaja, C.; Curigliano, G.; Tarantino, P. Targeting HER3 for cancer treatment: A new horizon for an old target. *ESMO Open* **2023**, *8*, 100790. [CrossRef]

155. Berghoff, A.S.; Bartsch, R.; Preusser, M.; Ricken, G.; Steger, G.G.; Bago-Horvath, Z.; Rudas, M.; Streubel, B.; Dubsky, P.; Gnant, M.; et al. Co-overexpression of HER2/HER3 is a predictor of impaired survival in breast cancer patients. *Breast* **2014**, *23*, 637–643. [CrossRef]
156. Ogden, A.; Bhattarai, S.; Sahoo, B.; Mongan, N.P.; Alsaleem, M.; Green, A.R.; Aleskandarany, M.; Ellis, I.O.; Pattni, S.; Li, X.; et al. Combined HER3-EGFR score in triple-negative breast cancer provides prognostic and predictive significance superior to individual biomarkers. *Sci. Rep.* **2020**, *10*, 3009. [CrossRef] [PubMed]
157. Bensch, F.; Lamberts, L.E.; Smeenk, M.M.; Jorritsma-Smit, A.; Lub-de Hooge, M.N.; Terwisscha van Scheltinga, A.G.T.; de Jong, J.R.; Gietema, J.A.; Schröder, C.P.; Thomas, M.; et al. (89)Zr-Lumretuzumab PET Imaging before and during HER3 Antibody Lumretuzumab Treatment in Patients with Solid Tumors. *Clin. Cancer Res.* **2017**, *23*, 6128–6137. [CrossRef] [PubMed]
158. Menke-van der Houven van Oordt, C.W.; McGeoch, A.; Bergstrom, M.; McSherry, I.; Smith, D.A.; Cleveland, M.; Al-Azzam, W.; Chen, L.; Verheul, H.; Hoekstra, O.S.; et al. Immuno-PET Imaging to Assess Target Engagement: Experience from (89)Zr-Anti-HER3 mAb (GSK2849330) in Patients with Solid Tumors. *J. Nucl. Med.* **2019**, *60*, 902–909. [CrossRef]
159. Pool, M.; Kol, A.; de Jong, S.; de Vries, E.G.E.; Lub-de Hooge, M.N.; Terwisscha van Scheltinga, A.G.T. (89)Zr-mAb3481 PET for HER3 tumor status assessment during lapatinib treatment. *MAbs* **2017**, *9*, 1370–1378. [CrossRef]
160. Wehrenberg-Klee, E.; Turker, N.S.; Heidari, P.; Larimer, B.; Juric, D.; Baselga, J.; Scaltriti, M.; Mahmood, U. Differential Receptor Tyrosine Kinase PET Imaging for Therapeutic Guidance. *J. Nucl. Med.* **2016**, *57*, 1413–1419. [CrossRef]
161. Rinne, S.S.; Leitao, C.D.; Abouzayed, A.; Vorobyeva, A.; Tolmachev, V.; Ståhl, S.; Löfblom, J.; Orlova, A. HER3 PET Imaging: (68)Ga-Labeled Affibody Molecules Provide Superior HER3 Contrast to (89)Zr-Labeled Antibody and Antibody-Fragment-Based Tracers. *Cancers* **2021**, *13*, 4791. [CrossRef] [PubMed]
162. Rosestedt, M.; Andersson, K.G.; Mitran, B.; Tolmachev, V.; Löfblom, J.; Orlova, A.; Ståhl, S. Affibody-mediated PET imaging of HER3 expression in malignant tumours. *Sci. Rep.* **2015**, *5*, 15226. [CrossRef] [PubMed]
163. Da Pieve, C.; Allott, L.; Martins, C.D.; Vardon, A.; Ciobota, D.M.; Kramer-Marek, G.; Smith, G. Efficient [(18)F]AlF Radiolabeling of ZHER3:8698 Affibody Molecule for Imaging of HER3 Positive Tumors. *Bioconjugate Chem.* **2016**, *27*, 1839–1849. [CrossRef]
164. Martins, C.D.; Da Pieve, C.; Burley, T.A.; Smith, R.; Ciobota, D.M.; Allott, L.; Harrington, K.J.; Oyen, W.J.G.; Smith, G.; Kramer-Marek, G. HER3-Mediated Resistance to Hsp90 Inhibition Detected in Breast Cancer Xenografts by Affibody-Based PET Imaging. *Clin. Cancer Res.* **2018**, *24*, 1853–1865. [CrossRef] [PubMed]
165. Wehrenberg-Klee, E.; Sinevici, N.; Nesti, S.; Kalomeris, T.; Austin, E.; Larimer, B.; Mahmood, U. HER3 PET Imaging Identifies Dynamic Changes in HER3 in Response to HER2 Inhibition with Lapatinib. *Mol. Imaging Biol.* **2021**, *23*, 930–940. [CrossRef] [PubMed]
166. Liu, Y.; Tamimi, R.M.; Collins, L.C.; Schnitt, S.J.; Gilmore, H.L.; Connolly, J.L.; Colditz, G.A. The association between vascular endothelial growth factor expression in invasive breast cancer and survival varies with intrinsic subtypes and use of adjuvant systemic therapy: Results from the Nurses' Health Study. *Breast Cancer Res. Treat.* **2011**, *129*, 175–184. [CrossRef] [PubMed]
167. Nasir, A.; Holzer, T.R.; Chen, M.; Man, M.Z.; Schade, A.E. Differential expression of VEGFR2 protein in HER2 positive primary human breast cancer: Potential relevance to anti-angiogenic therapies. *Cancer Cell Int.* **2017**, *17*, 56. [CrossRef]
168. Brogowska, K.K.; Zajkowska, M.; Mroczko, B. Vascular Endothelial Growth Factor Ligands and Receptors in Breast Cancer. *J. Clin. Med.* **2023**, *12*, 2412. [CrossRef] [PubMed]
169. Sun, Z.; Lan, X.; Xu, S.; Li, S.; Xi, Y. Efficacy of bevacizumab combined with chemotherapy in the treatment of HER2-negative metastatic breast cancer: A network meta-analysis. *BMC Cancer* **2020**, *20*, 180. [CrossRef] [PubMed]
170. Zhu, X.; Zhou, W. The Emerging Regulation of VEGFR-2 in Triple-Negative Breast Cancer. *Front. Endocrinol.* **2015**, *6*, 159. [CrossRef] [PubMed]
171. Ayoub, N.M.; Jaradat, S.K.; Al-Shami, K.M.; Alkhalifa, A.E. Targeting Angiogenesis in Breast Cancer: Current Evidence and Future Perspectives of Novel Anti-Angiogenic Approaches. *Front. Pharmacol.* **2022**, *13*, 838133. [CrossRef] [PubMed]
172. Gaykema, S.B.; Brouwers, A.H.; Lub-de Hooge, M.N.; Pleijhuis, R.G.; Timmer-Bosscha, H.; Pot, L.; van Dam, G.M.; van der Meulen, S.B.; de Jong, J.R.; Bart, J.; et al. 89Zr-bevacizumab PET imaging in primary breast cancer. *J. Nucl. Med.* **2013**, *54*, 1014–1018. [CrossRef] [PubMed]
173. Terwisscha van Scheltinga, A.G.; Berghuis, P.; Nienhuis, H.H.; Timmer-Bosscha, H.; Pot, L.; Gaykema, S.B.; Lub-de Hooge, M.N.; Kosterink, J.G.; de Vries, E.G.; Schröder, C.P. Visualising dual downregulation of insulin-like growth factor receptor-1 and vascular endothelial growth factor-A by heat shock protein 90 inhibition effect in triple negative breast cancer. *Eur. J. Cancer* **2014**, *50*, 2508–2516. [CrossRef] [PubMed]
174. Yang, Q.; Chen, Z.; Qiu, Y.; Huang, W.; Wang, T.; Song, L.; Sun, X.; Li, C.; Xu, X.; Kang, L. Theranostic role of (89)Zr- and (177)Lu-labeled aflibercept in breast cancer. *Eur. J. Nucl. Med. Mol. Imaging* **2024**, *51*, 1246–1260. [CrossRef]
175. Wang, H.; Cai, W.; Chen, K.; Li, Z.B.; Kashefi, A.; He, L.; Chen, X. A new PET tracer specific for vascular endothelial growth factor receptor 2. *Eur. J. Nucl. Med. Mol. Imaging* **2007**, *34*, 2001–2010. [CrossRef]
176. Zhang, Y.; Hong, H.; Niu, G.; Valdovinos, H.F.; Orbay, H.; Nayak, T.R.; Chen, X.; Barnhart, T.E.; Cai, W. Positron emission tomography imaging of vascular endothelial growth factor receptor expression with (61)Cu-labeled lysine-tagged VEGF121. *Mol. Pharm.* **2012**, *9*, 3586–3594. [CrossRef]
177. Meyer, J.P.; Edwards, K.J.; Kozlowski, P.; Backer, M.V.; Backer, J.M.; Lewis, J.S. Selective Imaging of VEGFR-1 and VEGFR-2 Using 89Zr-Labeled Single-Chain VEGF Mutants. *J. Nucl. Med.* **2016**, *57*, 1811–1816. [CrossRef] [PubMed]

178. Tekabe, Y.; Rodrigues, K.; Li, Q.; Backer, M.; Backer, J.; Johnson, L. VEGF receptor specific imaging in atherosclerotic lesions in diabetic and non-diabetic ApoE -/- mice. *J. Nucl. Med.* **2016**, *57*, 1648.
179. Cai, W.; Guzman, R.; Hsu, A.R.; Wang, H.; Chen, K.; Sun, G.; Gera, A.; Choi, R.; Bliss, T.; He, L.; et al. Positron Emission Tomography Imaging of Poststroke Angiogenesis. *Stroke* **2009**, *40*, 270–277. [CrossRef]
180. Collins, L.C.; Cole, K.S.; Marotti, J.D.; Hu, R.; Schnitt, S.J.; Tamimi, R.M. Androgen receptor expression in breast cancer in relation to molecular phenotype: Results from the Nurses' Health Study. *Mod. Pathol.* **2011**, *24*, 924–931. [CrossRef]
181. Park, S.; Koo, J.S.; Kim, M.S.; Park, H.S.; Lee, J.S.; Lee, J.S.; Kim, S.I.; Park, B.W.; Lee, K.S. Androgen receptor expression is significantly associated with better outcomes in estrogen receptor-positive breast cancers. *Ann. Oncol.* **2011**, *22*, 1755–1762. [CrossRef] [PubMed]
182. Anestis, A.; Zoi, I.; Papavassiliou, A.G.; Karamouzis, M.V. Androgen Receptor in Breast Cancer-Clinical and Preclinical Research Insights. *Molecules* **2020**, *25*, 358. [CrossRef]
183. Dass, S.A.; Tan, K.L.; Selva Rajan, R.; Mokhtar, N.F.; Mohd Adzmi, E.R.; Wan Abdul Rahman, W.F.; Tengku Din, T.; Balakrishnan, V. Triple Negative Breast Cancer: A Review of Present and Future Diagnostic Modalities. *Medicina* **2021**, *57*, 62. [CrossRef] [PubMed]
184. Venema, C.M.; Mammatas, L.H.; Schröder, C.P.; van Kruchten, M.; Apollonio, G.; Glaudemans, A.; Bongaerts, A.H.H.; Hoekstra, O.S.; Verheul, H.M.W.; Boven, E.; et al. Androgen and Estrogen Receptor Imaging in Metastatic Breast Cancer Patients as a Surrogate for Tissue Biopsies. *J. Nucl. Med.* **2017**, *58*, 1906–1912. [CrossRef] [PubMed]
185. Boers, J.; Venema, C.M.; de Vries, E.F.J.; Hospers, G.A.P.; Boersma, H.H.; Rikhof, B.; Dorbritz, C.; Glaudemans, A.; Schröder, C.P. Serial [(18)F]-FDHT-PET to predict bicalutamide efficacy in patients with androgen receptor positive metastatic breast cancer. *Eur. J. Cancer* **2021**, *144*, 151–161. [CrossRef] [PubMed]
186. Jacene, H.; Liu, M.; Cheng, S.C.; Abbott, A.; Dubey, S.; McCall, K.; Young, D.; Johnston, M.; Van den Abbeele, A.D.; Overmoyer, B. Imaging Androgen Receptors in Breast Cancer with (18)F-Fluoro-5α-Dihydrotestosterone PET: A Pilot Study. *J. Nucl. Med.* **2022**, *63*, 22–28. [CrossRef] [PubMed]
187. Antunes, I.F.; Dost, R.J.; Hoving, H.D.; van Waarde, A.; Dierckx, R.; Samplonius, D.F.; Helfrich, W.; Elsinga, P.H.; de Vries, E.F.J.; de Jong, I.J. Synthesis and Evaluation of (18)F-Enzalutamide, a New Radioligand for PET Imaging of Androgen Receptors: A Comparison with 16β-(18)F-Fluoro-5α-Dihydrotestosterone. *J. Nucl. Med.* **2021**, *62*, 1140–1145. [CrossRef]
188. Jia, M.; Dahlman-Wright, K.; Gustafsson, J.-Å. Estrogen receptor alpha and beta in health and disease. *Best. Pract. Res. Clin. Endocrinol. Metab.* **2015**, *29*, 557–568. [CrossRef]
189. Huang, B.; Omoto, Y.; Iwase, H.; Yamashita, H.; Toyama, T.; Coombes, R.C.; Filipovic, A.; Warner, M.; Gustafsson, J. Differential expression of estrogen receptor α, β1, and β2 in lobular and ductal breast cancer. *Proc. Natl. Acad. Sci. USA* **2014**, *111*, 1933–1938. [CrossRef] [PubMed]
190. Marotti, J.D.; Collins, L.C.; Hu, R.; Tamimi, R.M. Estrogen receptor-beta expression in invasive breast cancer in relation to molecular phenotype: Results from the Nurses' Health Study. *Mod. Pathol.* **2010**, *23*, 197–204. [CrossRef]
191. Choi, Y. Estrogen Receptor β Expression and Its Clinical Implication in Breast Cancers: Favorable or Unfavorable? *J. Breast Cancer* **2022**, *25*, 75–93. [CrossRef]
192. Sellitto, A.; D'Agostino, Y.; Alexandrova, E.; Lamberti, J.; Pecoraro, G.; Memoli, D.; Rocco, D.; Coviello, E.; Giurato, G.; Nassa, G.; et al. Insights into the Role of Estrogen Receptor β in Triple-Negative Breast Cancer. *Cancers* **2020**, *12*, 1477. [CrossRef] [PubMed]
193. Yan, S.; Wang, J.; Chen, H.; Zhang, D.; Imam, M. Divergent features of ERβ isoforms in triple negative breast cancer: Progress and implications for further research. *Front. Cell Dev. Biol.* **2023**, *11*, 1240386. [CrossRef]
194. Yoo, J.; Dence, C.S.; Sharp, T.L.; Katzenellenbogen, J.A.; Welch, M.J. Synthesis of an estrogen receptor beta-selective radioligand: 5-[18F]fluoro-(2R,3S)-2,3-bis(4-hydroxyphenyl)pentanenitrile and comparison of in vivo distribution with 16alpha-[18F]fluoro-17beta-estradiol. *J. Med. Chem.* **2005**, *48*, 6366–6378. [CrossRef] [PubMed]
195. Zhou, Y.; Lei, P.; Han, J.; Wang, Z.; Ji, A.; Wu, Y.; Zheng, L.; Zhang, X.; Qu, C.; Min, J.; et al. Development of a Novel (18)F-Labeled Probe for PET Imaging of Estrogen Receptor β. *J. Med. Chem.* **2023**, *66*, 1210–1220. [CrossRef] [PubMed]
196. Antunes, I.F.; Willemsen, A.T.M.; Sijbesma, J.W.A.; Boerema, A.S.; van Waarde, A.; Glaudemans, A.; Dierckx, R.; de Vries, E.G.E.; Hospers, G.A.P.; de Vries, E.F.J. In Vivo Quantification of ERβ Expression by Pharmacokinetic Modeling: Studies with (18)F-FHNP PET. *J. Nucl. Med.* **2017**, *58*, 1743–1748. [CrossRef]
197. Krishnakumar, R.; Kraus, W.L. The PARP side of the nucleus: Molecular actions, physiological outcomes, and clinical targets. *Mol. Cell* **2010**, *39*, 8–24. [CrossRef] [PubMed]
198. Ledermann, J.; Harter, P.; Gourley, C.; Friedlander, M.; Vergote, I.; Rustin, G.; Scott, C.L.; Meier, W.; Shapira-Frommer, R.; Safra, T.; et al. Olaparib maintenance therapy in patients with platinum-sensitive relapsed serous ovarian cancer: A preplanned retrospective analysis of outcomes by BRCA status in a randomised phase 2 trial. *Lancet Oncol.* **2014**, *15*, 852–861. [CrossRef] [PubMed]
199. Mazzotta, A.; Partipilo, G.; De Summa, S.; Giotta, F.; Simone, G.; Mangia, A. Nuclear PARP1 expression and its prognostic significance in breast cancer patients. *Tumor Biol.* **2016**, *37*, 6143–6153. [CrossRef] [PubMed]
200. Domagala, P.; Huzarski, T.; Lubinski, J.; Gugala, K.; Domagala, W. PARP-1 expression in breast cancer including BRCA1-associated, triple negative and basal-like tumors: Possible implications for PARP-1 inhibitor therapy. *Breast Cancer Res. Treat.* **2011**, *127*, 861–869. [CrossRef]

201. Stanley, J.; Klepczyk, L.; Keene, K.; Wei, S.; Li, Y.; Forero, A.; Grizzle, W.; Wielgos, M.; Brazelton, J.; LoBuglio, A.F.; et al. PARP1 and phospho-p65 protein expression is increased in human HER2-positive breast cancers. *Breast Cancer Res. Treat.* **2015**, *150*, 569–579. [CrossRef] [PubMed]
202. Sklias, T.; Vardas, V.; Pantazaka, E.; Christopoulou, A.; Georgoulias, V.; Kotsakis, A.; Vasilopoulos, Y.; Kallergi, G. PARP-1 Expression and BRCA1 Mutations in Breast Cancer Patients' CTCs. *Cancers* **2022**, *14*, 1731. [CrossRef] [PubMed]
203. Zhou, D.; Chu, W.; Xu, J.; Jones, L.A.; Peng, X.; Li, S.; Chen, D.L.; Mach, R.H. Synthesis, [^{18}F] radiolabeling, and evaluation of poly (ADP-ribose) polymerase-1 (PARP-1) inhibitors for in vivo imaging of PARP-1 using positron emission tomography. *Bioorganic Med. Chem.* **2014**, *22*, 1700–1707. [CrossRef] [PubMed]
204. Edmonds, C.E.; Makvandi, M.; Lieberman, B.P.; Xu, K.; Zeng, C.; Li, S.; Hou, C.; Lee, H.; Greenberg, R.A.; Mankoff, D.A.; et al. [(18)F]FluorThanatrace uptake as a marker of PARP1 expression and activity in breast cancer. *Am. J. Nucl. Med. Mol. Imaging* **2016**, *6*, 94–101.
205. McDonald, E.S.; Pantel, A.R.; Shah, P.D.; Farwell, M.D.; Clark, A.S.; Doot, R.K.; Pryma, D.A.; Carlin, S.D. In vivo visualization of PARP inhibitor pharmacodynamics. *JCI Insight* **2021**, *6*, e146592. [CrossRef]
206. Xu, J.; Chen, H.; Rogers, B.E.; Katzenellenbogen, J.A.; Zhou, D. Solid phase radiosynthesis of an olaparib derivative using 4-[(18)F] fluorobenzoic acid and in vivo evaluation in breast and prostate cancer xenograft models for PARP-1 expression. *Nucl. Med. Biol.* **2022**, *114–115*, 65–70. [CrossRef]
207. Stotz, S.; Kinzler, J.; Nies, A.T.; Schwab, M.; Maurer, A. Two experts and a newbie: [(18)F]PARPi vs [(18)F]FTT vs [(18)F]FPyPARP-a comparison of PARP imaging agents. *Eur. J. Nucl. Med. Mol. Imaging* **2022**, *49*, 834–846. [CrossRef] [PubMed]
208. Bowden, G.D.; Stotz, S.; Kinzler, J.; Geibel, C.; Lämmerhofer, M.; Pichler, B.J.; Maurer, A. DoE Optimization Empowers the Automated Preparation of Enantiomerically Pure [(18)F]Talazoparib and its In Vivo Evaluation as a PARP Radiotracer. *J. Med. Chem.* **2021**, *64*, 15690–15701. [CrossRef]
209. Shuhendler, A.J.; Cui, L.; Chen, Z.; Shen, B.; Chen, M.; James, M.L.; Witney, T.H.; Bazalova-Carter, M.; Gambhir, S.S.; Chin, F.T.; et al. [(18)F]-SuPAR: A Radiofluorinated Probe for Noninvasive Imaging of DNA Damage-Dependent Poly(ADP-ribose) Polymerase Activity. *Bioconjugate Chem.* **2019**, *30*, 1331–1342. [CrossRef] [PubMed]
210. Zheng, W.; Huang, Y.; Xie, Y.; Yang, T.; Cheng, X.; Chen, H.; Li, C.; Jiang, Z.; Yu, Z.; Li, Z.; et al. Design, Synthesis, and Evaluation of [(18)F]BIBD-300 as a Positron Emission Tomography Tracer for Poly(ADP-Ribose) Polymerase-1. *Mol. Pharm.* **2024**, *21*, 2606–2621. [CrossRef]
211. Stanton, S.E.; Disis, M.L. Clinical significance of tumor-infiltrating lymphocytes in breast cancer. *J. Immunother. Cancer* **2016**, *4*, 59. [CrossRef]
212. Alkhayyal, N.; Elemam, N.M.; Hussein, A.; Magdub, S.; Jundi, M.; Maghazachi, A.A.; Talaat, I.M.; Bendardaf, R. Expression of immune checkpoints (PD-L1 and IDO) and tumour-infiltrating lymphocytes in breast cancer. *Heliyon* **2022**, *8*, e10482. [CrossRef]
213. Adams, S.; Schmid, P.; Rugo, H.S.; Winer, E.P.; Loirat, D.; Awada, A.; Cescon, D.W.; Iwata, H.; Campone, M.; Nanda, R.; et al. Pembrolizumab monotherapy for previously treated metastatic triple-negative breast cancer: Cohort A of the phase II KEYNOTE-086 study. *Ann. Oncol.* **2019**, *30*, 397–404. [CrossRef] [PubMed]
214. Huo, X.; Shen, G.; Liu, Z.; Liang, Y.; Li, J.; Zhao, F.; Ren, D.; Zhao, J. Addition of immunotherapy to chemotherapy for metastatic triple-negative breast cancer: A systematic review and meta-analysis of randomized clinical trials. *Crit. Rev. Oncol. Hematol.* **2021**, *168*, 103530. [CrossRef] [PubMed]
215. Massicano, A.V.F.; Song, P.N.; Mansur, A.; White, S.L.; Sorace, A.G.; Lapi, S.E. [(89)Zr]-Atezolizumab-PET Imaging Reveals Longitudinal Alterations in PDL1 during Therapy in TNBC Preclinical Models. *Cancers* **2023**, *15*, 2708. [CrossRef] [PubMed]
216. Bensch, F.; van der Veen, E.L.; Lub-de Hooge, M.N.; Jorritsma-Smit, A.; Boellaard, R.; Kok, I.C.; Oosting, S.F.; Schröder, C.P.; Hiltermann, T.J.N.; van der Wekken, A.J.; et al. (89)Zr-atezolizumab imaging as a non-invasive approach to assess clinical response to PD-L1 blockade in cancer. *Nat. Med.* **2018**, *24*, 1852–1858. [CrossRef] [PubMed]
217. Jagoda, E.M.; Vasalatiy, O.; Basuli, F.; Opina, A.C.L.; Williams, M.R.; Wong, K.; Lane, K.C.; Adler, S.; Ton, A.T.; Szajek, L.P.; et al. Immuno-PET Imaging of the Programmed Cell Death-1 Ligand (PD-L1) Using a Zirconium-89 Labeled Therapeutic Antibody, Avelumab. *Mol. Imaging* **2019**, *18*, 1536012119829986. [CrossRef] [PubMed]
218. Li, M.; Ehlerding, E.B.; Jiang, D.; Barnhart, T.E.; Chen, W.; Cao, T.; Engle, J.W.; Cai, W. In vivo characterization of PD-L1 expression in breast cancer by immuno-PET with (89)Zr-labeled avelumab. *Am. J. Transl. Res.* **2020**, *12*, 1862–1872. [PubMed]
219. Xu, M.; Han, Y.; Liu, G.; Xu, Y.; Duan, D.; Liu, H.; Du, F.; Luo, P.; Liu, Z. Preclinical Study of a Fully Human Anti-PD-L1 Antibody as a Theranostic Agent for Cancer Immunotherapy. *Mol. Pharm.* **2018**, *15*, 4426–4433. [CrossRef]
220. Malih, S.; Lin, W.; Tang, Z.; DeLuca, M.C.; Engle, J.W.; Alirezapour, B.; Cai, W.; Rasaee, M.J. Noninvasive PET imaging of tumor PD-L1 expression with (64)Cu-labeled Durvalumab. *Am. J. Nucl. Med. Mol. Imaging* **2024**, *14*, 31–40. [CrossRef]
221. Radaram, B.; Glazer, S.E.; Yang, P.; Li, C.W.; Hung, M.C.; Gammon, S.T.; Alauddin, M.; Piwnica-Worms, D. Evaluation of (89)Zr-Labeled Anti-PD-L1 Monoclonal Antibodies Using DFO and Novel HOPO Analogues as Chelating Agents for Immuno-PET. *ACS Omega* **2023**, *8*, 17181–17194. [CrossRef] [PubMed]
222. Yan, H.; Endo, Y.; Shen, Y.; Rotstein, D.; Dokmanovic, M.; Mohan, N.; Mukhopadhyay, P.; Gao, B.; Pacher, P.; Wu, W.J. Ado-Trastuzumab Emtansine Targets Hepatocytes Via Human Epidermal Growth Factor Receptor 2 to Induce Hepatotoxicity. *Mol. Cancer Ther.* **2016**, *15*, 480–490. [CrossRef] [PubMed]

223. Berchuck, A.; Kamel, A.; Whitaker, R.; Kerns, B.; Olt, G.; Kinney, R.; Soper, J.T.; Dodge, R.; Clarke-Pearson, D.L.; Marks, P.; et al. Overexpression of HER-2/neu is associated with poor survival in advanced epithelial ovarian cancer. *Cancer Res.* **1990**, *50*, 4087–4091. [PubMed]
224. Iqbal, R.; Yaqub, M.; Oprea-Lager, D.E.; Liu, Y.; Luik, A.M.; Beelen, A.P.; Schuit, R.C.; Windhorst, A.D.; Boellaard, R.; Menke-van der Houven van Oordt, C.W. Biodistribution of ¹⁸F-FES in Patients with Metastatic ER+ Breast Cancer Undergoing Treatment with Rintodestrant (G1T48), a Novel Selective ER Degrader. *J. Nucl. Med.* **2022**, *63*, 694–699. [CrossRef] [PubMed]
225. Szántó, M.; Gupte, R.; Kraus, W.L.; Pacher, P.; Bai, P. PARPs in lipid metabolism and related diseases. *Progress. Lipid Res.* **2021**, *84*, 101117. [CrossRef]